Cascading tipping points
on the dynamics of coupled critical transitions

Master's thesis by Mark M. Dekker
Institute for Marine and Atmospheric research Utrecht (IMAU)
Utrecht University

Student number: 3672271
E-mail: m.m.dekker@outlook.com
Date of presentation: July 4th 2017
Supervision: prof. dr. ir. H.A. Dijkstra and dr. A.S. von der Heydt

Abstract for the general public

We introduce the new concept of cascading tipping. It is defined as the event of an large change in a first, leading system, which through a domino effect makes another, following system, also undergo a large change. A mathematical framework is created, where we use simple models that show these phenomena. Four deterministic cascading event types are defined, called the (1) double-fold, (2) fold-Hopf, (3) Hopf-fold, and (4) double-Hopf cascade, based on which type of change the system undergoes. More subtle forms of cascading tipping are defined when we add small randomness (noise) to the models. Statistical analysis is applied on cascading tipping to see what happens during such a period and to try to find a signal that could warn us if such an event is about to happen. We apply this theory on two cases in the real climate system. The first case is concerned with a collapse of the ocean's overturning circulation down to a halted circulation in the northern hemisphere. Using cascading tipping theory, our conceptual models show that in certain conditions, such an event can lead to an intensification of El-Niño events and the oscillation associated with it. We verify this intensification using complex model output. The second case also concerns a large change in the ocean's overturning circulation, which may induce the onset of southern hemispheric land ice growth. These examples suggest the theoretical possibility of such events in the climate system.

Contents

1 Introduction **3**

2 Mathematical framework **4**
2.1 Bifurcating systems and critical thresholds . . . 4
2.1.1 Saddle-node bifurcations . . . 4
2.1.2 Hopf bifurcations . . . 4
2.2 Deterministic cascading tipping . . . 4
2.2.1 Type 1: Double fold cascade . . . 4
2.2.2 Type 2: Fold-Hopf cascade . . . 5
2.2.3 Type 3: Hopf-fold cascade . . . 6
2.2.4 Type 4: Double Hopf cascade . . . 6
2.3 Stochastic cascading tipping . . . 7

3 Statistical analysis of critical transitions **7**
3.1 Analyzing tipping points . . . 7
3.1.1 Degenerate fingerprinting . . . 8
3.1.2 Detrended fluctuation analysis . . . 8
3.2 Analyzing cascading tipping points . . . 8
3.2.1 Detrended cross-correlation analysis . . . 8
3.2.2 Extrapolation of the following DFA . . . 9
3.3 Simulations . . . 9
3.3.1 Double-fold cascading tipping . . . 9
3.3.2 Fold-Hopf cascading tipping . . . 11

4 Application 1: Meridional overturning and ENSO **12**
4.1 Model details . . . 13
4.1.1 Leading system - Meridional Overturning . . . 13
4.1.2 Following system - El-Niño Southern Oscillation . . . 14
4.2 Results . . . 14
4.3 Verification with complex model output . . . 15

5 Application 2: Meridional overturning and land ice **17**
5.1 Model details . . . 17
5.2 Results . . . 17
5.3 Two-step signal in δ^{18}O . . . 18

6 Summary and Conclusions **18**

Appendix A: Proofs concerning critical thresholds **19**

Abstract. We introduce the new concept of cascading tipping. It is defined as the event of a critical transition in a first, leading system, altering background conditions such that another critical transition in a second, following system occurs. A mathematical framework is created, where systems with saddle-node and Hopf bifurcations are used to investigate the behavior of systems involving abrupt transitions. Four deterministic cascading event types are defined, including the (1) double-fold, (2) fold-Hopf, (3) Hopf-fold and (4) double-Hopf cascade. Considering stochastic systems, we discussed the effect on the probability density function (PDF) and flickering effects, allowing for more subtle critical transitions. Statistical indicators and analysis tools for critical transitions are discussed, including the general theory of critical slowing down, degenerate fingerprinting and detrended fluctuation analysis (DFA). These are applied to the concept of cascading tipping in the form of detrended cross correlation analysis (DCCA) and a special case of extrapolation using the DFA of the following system. Using ensemble simulation runs, these statistical indicators are analyzed for the double-fold cascade and the fold-Hopf cascade. The concept of cascading tipping is applied to two climatological cases: (1) the overturning circulation coupled to El-Niño Southern Oscillation (ENSO) and (2) the overturning circulation coupled to southern hemispheric land ice formation. For the first case, we couple two conceptual models to show a case where a collapse of the overturning leads to an intensification of ENSO. In the second case, an existing conceptual box model is perturbed such that a transition from a southern sinking towards a thermohaline overturning state is followed by southern hemispheric land ice formation. These examples suggest the theoretical possibility of such events in the climate system.

1 Introduction

Critical transitions can be found in many aspects of the earth's climate system. Typical examples of these transitions in palaeoclimate records are found in the abrupt cooling of the Younger Dryas (Livina and Lenton, 2007), the desertification of the Sahel region (Kutzbach et al., 1996) and the Eocene-Oligocene transition (Tigchelaar et al., 2011). Also in today's climate and future projections, potential tipping points are found. The Atlantic meridional overturning circulation (AMOC) (Dijkstra and Weijer, 2005; Stommel, 1961; Huisman et al., 2009), Arctic sea ice (Bathiany et al., 2016b), monsoon patterns, atmospheric zonal flow (Barriopedro et al., 2006), vegetation cover (Hirota et al., 2011; Aleina et al., 2013) and more local systems like coral reefs and permafrost are discussed in this context, both from a theoretical point of view (Bathiany et al., 2016a), and by using complex model data (Drijfhout et al., 2015).

Although many tipping points have been analyzed elaborately in separate subsystems, less attention has been given to the interaction between these transitions. A transition in a first, *leading*, system may alter the background conditions of a second, *following*, system (Lenton and Williams, 2013), causing it to undergo critical transition, too. For example, when the AMOC collapses, precipitation patterns may change such that the equilibrium structure of the vegetation cover in the Amazon rainforest is shifted (Hirota et al., 2011; Aleina et al., 2013). This may result in another transition, concerned with forest growth or dieback. We refer to this process of coupled critical transitions as 'cascading tipping'. There are already studies devoted to the interaction of theoretically stochastic coupled multistable systems in networks, e.g. in Ashwin et al. (2017) and Creaser et al. (2017), defining types of domino effects based on the synchrony of the transition (escape times) in the various coupled network nodes. However, these papers focus on network dynamics and do not yet give a general perspective on the concept of cascading tipping. This is the focus of this paper.

From a theoretical point of view, one can think of several mechanisms in the earth's climate that can show cascading tipping events. An example is the influence of the overturning circulation on the trade winds (through meridional sea surface temperature gradients), that in turn influence the intensity of the El-Niño Southern Oscillation (ENSO). It is argued that a collapse of the overturning would intensify ENSO (Lenton and Williams, 2013; Timmermann et al., 2007; Dong and Sutton, 2007), while there are other effects that would weaken ENSO (Timmermann et al., 2005).

Another example is the coupling between the overturning circulation and land ice. At the Eocene-Oligocene transition, a two-step signal is found in the δ^{18}O isotopic ratio, which is attributed to a deep-sea temperature drop followed by the (slower) growth of the Antarctic Ice Sheet (AIS). The deep-sea temperature drop can be related to a switch in overturning state, as investigated in Tigchelaar et al. (2011). The ice sheet formation is argued to be driven by a decreased atmospheric CO_2 (Pearson et al., 2009). This rises the question to which extent the switch in overturning circulation (first tipping) might impact the atmospheric CO_2 and therefore indirectly drive the growth of the AIS (second tipping), forming a cascading tipping event.

In the last few years, there is growing interest to formulate statistical indicators and early warning signals of tipping points. A system close to critical transition shows features of a 'critical slowing down', which can be mathematically derived (Dakos et al., 2008; Scheffer et al., 2009), but is also rather intuitive: in the vicinity of the tipping point, the system slowly loses its ability to recover from small perturbations. This results in increased variance, autocorrelation and potentially also increased skewness and flickering (Scheffer et al., 2009). To quantify the actual threshold of a critical transition, two distinguishable methods are used. The first is degenerate fingerprinting, which quantifies the autocorrelation by fitting an autoregressive iterative function through the time series (Held and Kleinen, 2004; Thompson and Sieber, 2011). The second, arguably more suited for non-stationary

time series (Livina and Lenton, 2007), is detrended fluctuation analysis (DFA), where the average fluctuation function $F(s)$ of polynomial fits in segments of size s is fit to a power law $F(s) \propto s^{\alpha}$ (Peng et al., 1994). Both these methods result in a scalar that increases when approaching a tipping point, and a particular threshold when the tipping point is actually reached and the transition starts to take place.

Analyzing cascading tipping is different from regular tipping analysis, as simultaneously the autocorrelation of two time series and their interaction need to be analyzed. Podnobik and Stanley (2007) proposed an altered form of DFA to assess the cross correlation between two non-stationary time series and called this method detrended cross-correlation analysis (DCCA). In the computation of the fluctuation function, they used cross-covariance instead of auto-covariance and fit this to a power law. This concept is further extended by defining a coefficient ρ_{DCCA} that accounts for the autocovariance of the individual time series (Zhou, 2008; Yuan et al., 2015). However, no statistical analysis and indicators have yet been formulated for cascading tipping events, and an attempt to fill this gap is done in this paper.

In this paper, we introduce the concept of cascading tipping. We start with a mathematical framework to define critical transitions, coupling and cascading tipping, including the formulation of typical dynamical systems that show cascading tipping events (section 2). We continue with discussing the statistical indicators used to analyze critical transitions, and apply them to ensemble simulations (section 3). Then two applications of cascading tipping in climate dynamics are investigated: the potential cascading tipping mechanism between the AMOC and ENSO (section 4) and between the AMOC and the AIS, which refers to the Eocene-Oligocene transition (section 5).

2 Mathematical framework

Critical transitions come in various forms. While transitions in the AMOC implies the overturning to go from one equilibrium state towards another (Stommel, 1961), a critical transition in northern hemisphere atmospheric zonal flow (Tantet et al., 2015; Charney and DeVore, 1979) implies abrupt changes in the variance or probability density function (PDF). This section attempts to analyze (cascading) critical transitions in a mathematical framework. For the most part of this analysis, we retain to a deterministic approach for simplicity. Later in this section, we will turn to a stochastic approach.

2.1 Bifurcating systems and critical thresholds

The simulation of abrupt change in a dynamical system as a consequence of a small forcing involves the concept of bifurcations. Here, we focus on two types of bifurcations, the back-to-back saddle-node and the Hopf bifurcation, reflecting some of these transitions (Thompson and Stewart, 2002). Here, we analyze systems that contain these bifurcation points and we specify the critical thresholds to reach these points.

2.1.1 Saddle-node bifurcations

A general form for a system that has a back-to-back saddle-node bifurcation could be the following differential equation:

$$\frac{dx}{dt} = a_1 x^3 + a_2 x + a_3 \tag{1}$$

where a_i are constants with $i \in \{1,2,3\}$, x a certain 1-dimensional state variable and t time. To formulate the position of the bifurcation point in terms of the parameters a_i, we proof several characteristics of Eqn. 1 in Appendix A. The result is that there are multiple equilibria in the system if and only if $a_1 < 0$, $a_2 > 0$ and $|a_3| < \sqrt{\frac{4a_1^3 a_2^3}{27a_1^4}}$. This means that given the right a_1 and a_2, a saddle-node bifurcation can be found at $a_3 = \pm\sqrt{\frac{-4a_1^3 a_2^3}{27a_1^4}}$.

2.1.2 Hopf bifurcations

A general form for a system that has a Hopf bifurcation could be the following set of differential equations:

$$\begin{aligned} \frac{dx}{dt} &= a_1 y + a_2(a_3 - (x^2+y^2))x \\ \frac{dy}{dt} &= b_1 x + b_2(b_3 - (x^2+y^2))y \end{aligned} \tag{2}$$

where a_i and b_j are constants with $i,j \in \{1,2,3\}$, x and y are certain state variables and t time. In Appendix A, it is proven that the system in Eqn. 2 reaches a stable periodic solution when coming from a stable stationary equilibrium if and only if $a_1 b_1 < 0$ and $a_2 a_3 + b_2 b_3 = 0$.

2.2 Deterministic cascading tipping

Taking the step from single bifurcation points to cascading critical transitions, we need to extend the dynamical systems by defining a leading system and a following system in terms of state variables with own differential equations. Coupling these variables is essential to simulate the cascading effect, but note that the coupling should not be such that the leading and following systems are essentially one and the same system. We will now define various types of cascading tipping events, which in the current framework consist of combinations of saddle-node and Hopf bifurcations.

2.2.1 Type 1: Double fold cascade

The most intuitive system that has the potential to undergo a cascading tipping event is a system where both the leading and the following system have saddle-node bifurcations ('folds'). Analogous to system Eqn. 1, we define a general

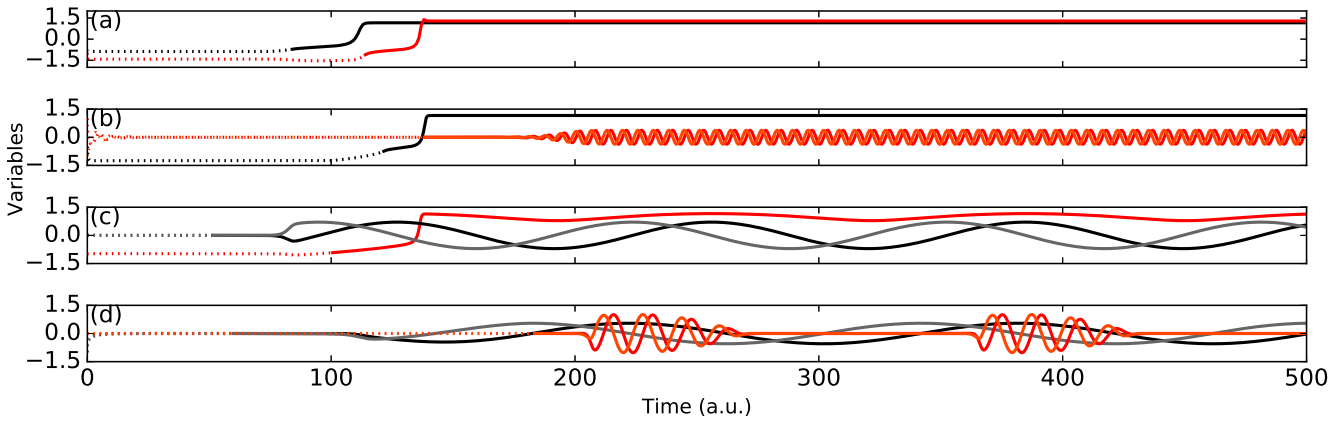

Figure 1. Example simulations for each cascading event type: the double-fold cascade (a), the fold-Hopf cascade (b), the Hopf-fold cascade (c) and the double Hopf cascade (d). Black and grey lines indicate the leading systems, red and orange lines indicate the following systems. Dotted lines indicate time before the critical threshold in the forcing $\phi(t)$ (black/grey) or coupling $\kappa(x)$ (red/orange) is reached, solid lines indicate the time after this.

form for this so-called double fold cascade as:

$$\begin{cases} \dfrac{dx}{dt} = a_1x^3 + a_2x + \phi \\ \dfrac{dy}{dt} = b_1y^3 + b_2y + \kappa(x) \end{cases} \tag{3}$$

where x is the leading system, y is the following system, a_i and b_i are constants, $\kappa(x) = \kappa_1 + \kappa_2 x$ is a coupling term (κ_1, κ_2 constants) between x and y and ϕ is a term which we can make time-dependent to apply a slow forcing on the system. When x is forced by $\phi(t)$ such that it reaches the limit point of the back-to-back saddle-node structure, y might also reach a limit point if the critical threshold of $|\kappa(x)| = \sqrt{\frac{4b_1^3b_2^3}{27b_1^4}}$ is attained (including $b_1 < 0$ and $b_2 > 0$). The above system is modelled and a resulting cascading tipping event is shown in Fig. 1a with parameter setting $\{a_1, a_2, b_1, b_2\} = \{-0.5, 0.5, -0.5, 1\}$ and $\kappa = 0.48x$. The system shown is forced by ϕ in the form of a ramp-function around the position of the bifurcation point of the leading system. This is also the case in the other types shown in Fig. 1. The back-to-back saddle-node structure of the leading system w.r.t. ϕ is visible in Fig. 2a, already showing the extra limitpoints that only affect the following system, of which the bifurcation structure is shown in Fig. 2e. The latter shows the existence of a regime (in ϕ) where there are four possible stable equilibria of the system.

A typical climatological example of such a cascading tipping event is the case of a collapsing overturning circulation, leading to a critical transition in the vegetation mass in the Amazon rainforest. The forcing $\phi(t)$ of the leading system is then the freshwater flux, and the coupling κ between the systems is done through precipitation patterns via the meridional sea surface temperature (SST) gradient. Both transitions imply a significant equilibrium shift, which is possible as multiple equilibria exist in these systems (Stommel, 1961; Aleina et al., 2013).

2.2.2 Type 2: Fold-Hopf cascade

The second category of cascading tipping events involves a fold bifurcation in the leading system and a subsequent Hopf bifurcation in the following system. Using analogous notation as in Eqn. 3, we present a general system that may produce this so-called fold-Hopf cascade:

$$\begin{cases} \dfrac{dx}{dt} = a_1x^3 + a_2x + \phi \\ \dfrac{dy}{dt} = b_1z + b_2(\kappa(x) - (y^2 + z^2))y \\ \dfrac{dz}{dt} = c_1y + c_2(\kappa(x) - (y^2 + z^2))z \end{cases} \tag{4}$$

where x is again the leading system, but now y and z together form the following system. If we make ϕ time-dependent to force x such that it is forced onto another equilibrium state, $\kappa(x)$ might cross 0 such that $\kappa(x)(b_2 + c_2) = 0$ and thus Hopf bifurcation is reached in (y, z). The resulting cascading tipping event is illustrated in Fig. 1b with parameter setting $\{a_1, a_2, b_1, b_2, c_1, c_2\} = \{-1, 1, 1, 1, -1, 1\}$ and $\kappa = -0.1 + 0.12x$. The back-to-back saddle-node is visible in Fig. 2b, but with an oscillatory regime in the upper branch (although the leading system itself does not oscillate, visible in the zero-amplitude). The Hopf bifurcation and subsequent non-zero amplitudes of an oscillation are visible in Fig. 2f, where in contrast to the bifurcation diagram of a system like Eqn. 2, a stable stationary equilibria are found on both sides of the Hopf bifurcation, as determined by the leading system's state.

An example of such a cascading event can be found in the hypothetical case where a collapse of the overturning cir-

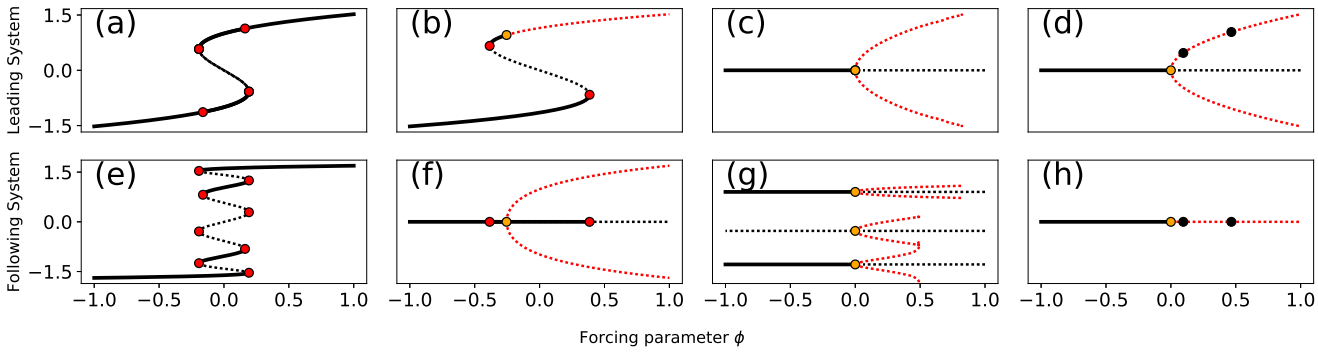

Figure 2. Bifurcation diagrams of the various cascading tipping types. Top: leading systems versus forcing $\phi(t)$. Bottom: following systems versus forcing $\phi(t)$. Lines indicate stable equilibria (black solid), instable equilibria (black dashed) and oscillatory equilibria (red dashed, non-zero amplitudes shown in pairs). Dots indicate important bifurcation points: limit points (red) Hopf bifurcation points (orange) and torus bifurcation points (black).

culation leads to an arising or strong weakening of El-Niño phenomena. The overturning is forced by the freshwater flux and the coupling with the Pacific ocean is found in the trade winds (Timmermann et al., 2007).

2.2.3 Type 3: Hopf-fold cascade

Cascading tipping category 3 involves a Hopf bifurcation in the leading system and a subsequent fold in the following system. Using analogous notation as before, we introduce a general form for this so-called Hopf-fold cascade:

$$\begin{cases} \dfrac{dx}{dt} = a_1 y + a_2(\phi - (x^2+y^2))x \\ \dfrac{dy}{dt} = b_1 x + b_2(\phi - (x^2+y^2))y \\ \dfrac{dz}{dt} = c_1 z^3 + c_2 z + \kappa(x) \end{cases} \tag{5}$$

where (x,y) together form the leading system, and z is the following system. Again, we can slowly increase ϕ such that the leading system (x,y) crosses a Hopf bifurcation ($\phi(t)(a_2+b_2)=0$), which may result in $\kappa(x)$ crossing $\sqrt{\frac{4c_1^3c_2^3}{27c_1^4}}$ such that a fold is reached in z. The above system is modelled and a resulting cascading tipping event is shown in Fig. 1c with parameter setting $\{a_1,a_2,b_1,b_2,c_1,c_2\} = \{0.05,1,-0.05,1,-1,1\}$ and $\kappa = 0.05+0.5x$. Note that this type of cascading tipping can come in various forms, which can be explained by looking at the bifurcation diagrams of both the leading (Fig. 2c) and the following (Fig. 2g) system. When ϕ is such that an oscillation starts in the leading system, the following system might also start oscillating a bit (visible in Fig. 2g). However, this is due to the changing position of the stable stationary equilibrium branch in the following system, not because of an intrinsic Hopf bifurcation, which within our framework means that the following system did not critically transit yet. If the amplitude of the leading system becomes large enough (e.g. when ϕ is increased further), the following system might be reduced to having only one stable equilibrium (visible in Fig. 2g as the stopping of the small oscillations in the lower branches). However, when the oscillation in the leading system becomes even larger, the leading system sweeps the following system between two equilibria: in the positive phase, the following system remains around the upper branch in Fig. 2g, in the negative phase, it is around the lower branch.

An example of such a cascading event is the opposite of the example used in the fold-Hopf cascade. The variability in ENSO can in turn also affect the equilibrium state of the MOC. If ENSO would stabilize, this has major consequences for precipitation patterns and heat fluxes that affect the meridional temperature gradient in the Atlantic. This in turn affects the meridional overturning and potentially forces a critical transition.

2.2.4 Type 4: Double Hopf cascade

The fourth and final category of cascading tipping discussed here involves a Hopf bifurcation in the leading system and a subsequent fold in the following system. Using analogous notation as above, we introduce a general form for this so-called double Hopf cascade:

$$\begin{cases} \dfrac{dx}{dt} = a_1 y + a_2(\phi - (x^2+y^2))x \\ \dfrac{dy}{dt} = b_1 x + b_2(\phi - (x^2+y^2))y \\ \dfrac{du}{dt} = c_1 v + c_2(\kappa(x) - (u^2+v^2))u \\ \dfrac{dv}{dt} = d_1 u + d_2(\kappa(x) - (u^2+v^2))v \end{cases} \tag{6}$$

where (x,y) together form the leading system, and (u,v) is the following system. If $\phi(t)$ forces (x,y) such that it a Hopf bifurcation point is reached ($\phi(a_2+b_2)=0$), $\kappa(x)$ might alter such that $\kappa(x)(c_2+d_2)$ reaches 0 and a Hopf bifurcation is crossed in (u,v). The

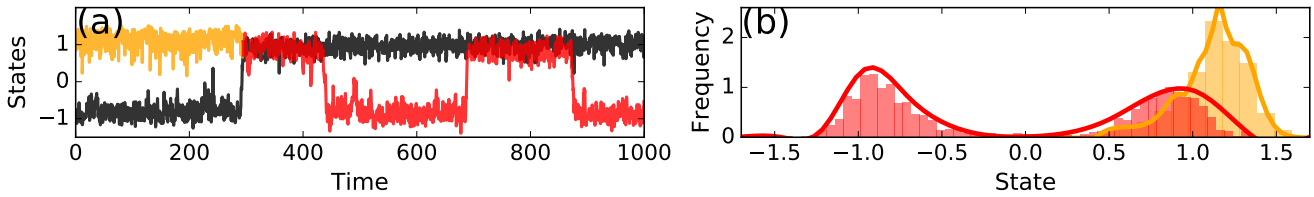

Figure 3. Example of stochastic tipping involving flickering. The leading system x is denoted in black, the following system is denoted in orange (before tipping of x) and red (after tipping of x). Left: time series of x and y, right: probability density functions of y before and after tipping.

resulting cascading tipping event is shown in Fig. 1d with parameter setting $\{a_1, a_2, b_1, b_2, c_1, c_2, d_1, d_2\} = \{0.04, 2, -0.04, 2, 0.4, 1, -0.4, 1\}$ and $\kappa = -0.05 + 2x$. It can be seen in the example that the position of the following system w.r.t. its Hopf bifurcation is periodic and therefore has some degree of reversibility. However, do note that (as shown in Fig. 1d), the periodicity in the leading system can be much slower than the one in the following system, making it temporarily irreversible. The equilibrium structures of the leading and following systems are shown in Fig. 2d and h, which indicate the presence of torus bifurcation points, reflecting the variable amplitude of the system's oscillations for specific values of ϕ.

An example of such a cascading event is the connection of the variability in ENSO with the variability in the Indian Ocean, or specifically, the Indian Ocean Dipole. Whenever ENSO attains increased variability (e.g. crosses a stochastic Hopf or period-doubling bifurcation), the Indian Ocean might do the same through these teleconnections. The connection between these systems is verified in coupled GCMs (Venzke et al., 2000).

2.3 Stochastic cascading tipping

The bifurcations as described in the above deterministic systems are also possible to occur in stochastic systems, although somewhat harder to predict due to the fact that internal variability (noise) rather than external forcing can make a system cross a bifurcation point, too. More specifically, subtle forms of tipping like flickering in regimes of multiple equilibria becomes possible, without altering background conditions. When considering cascading tipping, such an event might look like the one in Fig. 3, where the following system of equations is used:

$$\begin{cases} \dfrac{dx}{dt} = a_1 x^3 + a_2 x + \phi(t) + \zeta_x \\ \dfrac{dy}{dt} = b_1 y^3 + b_2 y + \kappa(x) + \zeta_y \end{cases} \tag{7}$$

which is the same system as in the case of the double fold cascade, but with added noise terms ζ_x and ζ_y. We use the parameters $\{a_1, a_2, b_1, b_2\} = \{-1, 1, -1, 1\}$, $\kappa = 0.5 - 0.5x$ and Gaussian white noise variance 0.8 (mean 0). Here, when the leading system x tips (black curve), the following system y does not directly following (orange and red curve), but comes into a state of multiple equilibria, where its variance allows for flickering, which has its impact on the probability density function (PDF) as seen in Fig. 3b. Although there is no direct bifurcation point reached, this can definitely be considered as an abrupt change or 'critical transition', as the PDF changes may have drastic consequences. Flickering between multiple states is seen in various systems of the earth's climate.

One can think of other stochastic variations of cascading tipping, especially when Hopf are concerned and the variance has a high magnitude with respect to the oscillation's amplitude. As there are a lot of individual variations without adding to the scope of this paper, we will not go into details here.

3 Statistical analysis of critical transitions

This section discusses the various tools to analyze single tipping events and proposes statistical indicators for the analysis of cascading tipping events.

3.1 Analyzing tipping points

We start with single tipping points. A system close to critical transition recovers more slowly from perturbations, which in turn increases memory in the time series. This lead to the theory of 'critical slowing down' prior to bifurcation points. The mathematical background and details are discussed in Scheffer et al. (2009), where they mainly focus on fold bifurcations, although they argue that this also occurs in systems involving Hopf bifurcations and even chaotic and spatially extended systems. The critical slowing down is expressed in increasing autocorrelation (often specified as the autoregressive coefficient at lag 1), increasing variance and increasing skewness. However, these indicators provide no early warning or critical threshold in the statistics of a time series whatsoever, and under certain conditions may not even be useful (Ditlevsen and Johnsen, 2010). This leads us to more complicated indicators discussed below.

3.1.1 Degenerate fingerprinting

As critical slowing down predicts increasing autoregressive behavior in the time series prior to a critical transition, the memory and thus influence of previous time steps towards later time steps is increased. After time-equidistant interpolation and detrending of the data, one can fit the following general autoregressive function to the series:

$$y_{n+1} = c \cdot y_n + \sigma \eta_n$$

or, in continuous form:

$$y(t) = y_0 \cdot c^t$$

where η_n is Gaussian white noise and $c = \exp(-\lambda \Delta t)$, where λ can be seen as the decay rate of perturbations in previous time steps. The variable c indicates this memory, becoming 1 when the series behaves like red noise, and becoming zero when the system behaves like white noise. This method is called degenerate fingerprinting (Thompson and Sieber, 2011). As the approaching of a bifurcation point involves an increase in memory, ultimately towards red noise behavior, the value of c is presumed to increase towards 1 when approaching a bifurcation point.

3.1.2 Detrended fluctuation analysis

A problem of degenerate fingerprinting is that it quickly captures shorter-time scale trends in the data. Detrended fluctuation analysis (DFA) is another method to analyze critical transitions, but copes well with non-stationarity while searching for long-range correlations (Peng et al., 1994; Livina and Lenton, 2007).

The procedure of DFA is as follows. First, we choose a window size s. Then, we divide the (cumulative-summed) time series in $N_s = N/s$ segments that do not overlap. In every window, the best polynomial fit of a chosen order is calculated. A quadratic polynomial is used here. The squared deviation from this quadratic polynomial for every window is summed, resulting in a measure of the auto-covariance fluctuating around the fit:

$$F^2(\nu, s) = \frac{1}{s} \sum_{i=1}^{s} [Y((\nu-1)s+i) - y_\nu(i)]^2 \tag{8}$$

with Y the detrended time series, y_ν the best polynomial fit in segment ν and N the length of the time series. Then, an average is taken over all segments to obtain the fluctuation function $F(s)$:

$$F(s) = \sqrt{\frac{1}{N/s} \sum_{\nu=1}^{N/s} F^2(\nu, s)} \tag{9}$$

which depends on s. We can now recognize long-range autocorrelations by fitting the fluctuation function to a power-law and looking at the resulting DFA-exponent α:

$$F(s) \propto s^\alpha \tag{10}$$

For $\alpha \leq 0.5$, there is no long-term correlation (fluctuations are white noise). However, when $\alpha > 0.5$, there are long-term correlations present. For $\alpha \geq 1.5$, the fluctuations act like red noise and the system has reached a bifurcation point. In stationary series, α is related to the auto-correlation exponent in $C(s) \propto s^{-\gamma}$.

Livina and Lenton (2007) proposed a DFA-propagator which is basically an empirically derived polynomial $\alpha(c)$ as function of the autoregressive propagator used degenerate fingerprinting. In the simulations done here, this turned out to be rather noisy and unpredictable, which is why we fitted the DFA scaling exponent explicitly for every (moving) window.

3.2 Analyzing cascading tipping points

Cascading tipping involves two systems with their own bifurcation structure and their proximity towards bifurcation points. Although the leading system may be close to tipping, the following system might still be far away from its bifurcation point and needs the critical transition of the leading system to even come close to this point. This is why the general measures for single tipping events cannot be used, nor can regular cross (Pearson) correlation due to the fact that the following and leading system do not have a one-to-one relationship (that would mean they are practically the same system), but are rather coupled in specific parameters, only seen in long-range correlations.

3.2.1 Detrended cross-correlation analysis

When approaching a cascading tipping point, the long-range cross-correlation between the two variables is expected to increase, because x becomes more auto-correlated and is less susceptible to noise, and therefore through the coupling influences y in a more robust way. To find long-range *cross*-correlations, a method so-called detrended cross-correlation analysis (DCCA) is developed during the past few years (Zebende, 2011; Podnobik and Stanley, 2007; Zhang et al., 2001; Zhou, 2008). Instead of taking the auto-covariance (Eqn. 8) to calculate the fluctuation function, one takes the cross-covariance:

$$\begin{aligned} F^2_{DCCA}(\nu, s) = & \frac{1}{s} \sum_{i=1}^{s} [(X((\nu-1)s+i) - x_\nu(i)) \\ & \cdot (Y((\nu-1)s+i) - y_\nu(i))]^2 \end{aligned} \tag{11}$$

with symbols analogous to Eqn. 8. With this function, one can calculate the fluctuation function and subsequent power-law scaling coefficient (Podnobik and Stanley, 2007; Zhang et al., 2001).

A variation on this is proposed by Zebende (2011) and involves the ratio between F^2_{DCCA} and F_{DFA} of the two systems. Specifically, one chooses a certain segment size s and computes:

$$\rho_{DCCA} = \frac{F^2_{DCCA}}{F_{DFA\{x\}} F_{DFA\{y\}}} \tag{12}$$

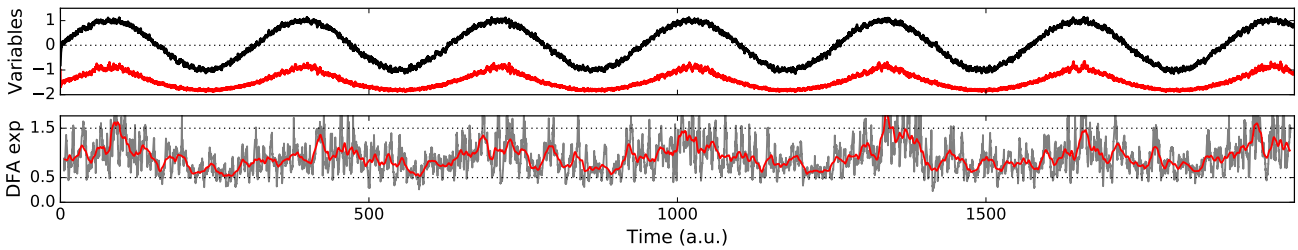

Figure 4. Example time series of system 13. Top: leading system x (black) and following system y (red). Bottom: DFA scaling exponent (grey shades; red indicates running mean).

which point towards the level of the long-term cross-correlation between variable x and y. It has values between -1 and 1.

3.2.2 Extrapolation of the following DFA

Because we know the DFA scaling exponent has a threshold of 1.5 that marks the position of the bifurcation point, an attempt to predict cascading tipping can also be figuring out for what state of the leading system, the following system attains DFA=1.5, and whether the leading system attains this state after a critical transition it is potentially close to. This involves the extrapolation of the relation between the state of the leading system and the DFA scaling exponent of the following system.

We illustrate this with an example using the following system:

$$\begin{cases} x(t) = & \sin(\frac{t}{50}) - x + \zeta_x \\ \frac{dy}{dt} = & y^3 - y + \kappa(x) + \zeta_y \end{cases} \tag{13}$$

with x the leading system, y the following system, $\kappa(x) = -2 + 2.2x$ a coupling term, ζ_x, ζ_y (Gaussian white, mean 0, variance 0.5) noise terms and t time. The large variability in x enables us to analyze the DFA of y at different levels of proximity towards its bifurcation point. The critical threshold of bifurcation in y is $\kappa(+\zeta_y) = \sqrt{\frac{-2}{1^3}} \approx 0.38$. When x is in the positive phase, this threshold is almost reached, forcing y close to its bifurcation point. In the negative phase of x, y leaves the multiple equilibria domain and remains in only one stable equilibrium with a broad potential function. These features can clearly be seen in Fig. 4, where the system is ran with $\Delta t = 0.1$, the Runge-Kutta fourth order integration method and a window size of 100. The distance of y towards its bifurcation point can be seen clearly in the DFA scaling exponent: values of 1.0-1.5 are reached in the positive phase (pointing towards long-range auto-correlations and the proximity of a bifurcation point) and 0.5-1.0 in the negative phase. To assess the relation between the state of x with the statistical indicators in y, Fig. 5 is made. The higher auto-correlation, variance, DFA propagator and DFA scaling coefficient in the positive phase of x are clearly visible. This confirms the theory of the DFA scaling exponent and its robustness.

This can also be used the other way around. When in two time series, a relation between the state of the first time series and DFA scaling exponent can be found, it is likely that the first could drive the second system to critical transition. When looking at Fig. 5f, one can almost see a linear relation between DFA_y and x. Extrapolating this gives an estimate x_0 for which the DFA_y becomes 1.5, or in other words, the value of the leading system for which the following system tips. Now, if we know from single-tipping early warnings that x is close to tipping, and we also know that the resulting leading system would go beyond x_0, we know that the system is close to cascading tipping. Although one should note that much variability is needed to make such a prediction accurate, this can be used as an early warning.

3.3 Simulations

The section above describes various diagnostic and prognostic tools to analyze cascading tipping. This section is devoted to give insight in the accuracy and the usefulness of the indicators. We will do this with respect to type 1 and type 2 cascading tipping.

3.3.1 Double-fold cascading tipping

We start with the double-fold cascade. To simulate these events and use statistical indicators, noise has to be included. The system of equations used here is:

$$\begin{cases} \frac{dx}{dt} = a_1 x^3 + a_2 x + \phi + \zeta_x \\ \frac{dy}{dt} = b_1 y^3 + b_2 y + \kappa(x) + \zeta_y \end{cases} \tag{14}$$

where x is the leading system, y the following system, a_i and b_i constant parameters, ϕ a time-dependent forcing, $\kappa(x)$ a x-dependent coupling and ζ_x, ζ_y Gaussian white noise terms. We simulate an ensemble of 10 runs with the parameter setting as displayed in Tab. 1 and initial conditions $(x_0, y_0) = (-0.8, -1)$.

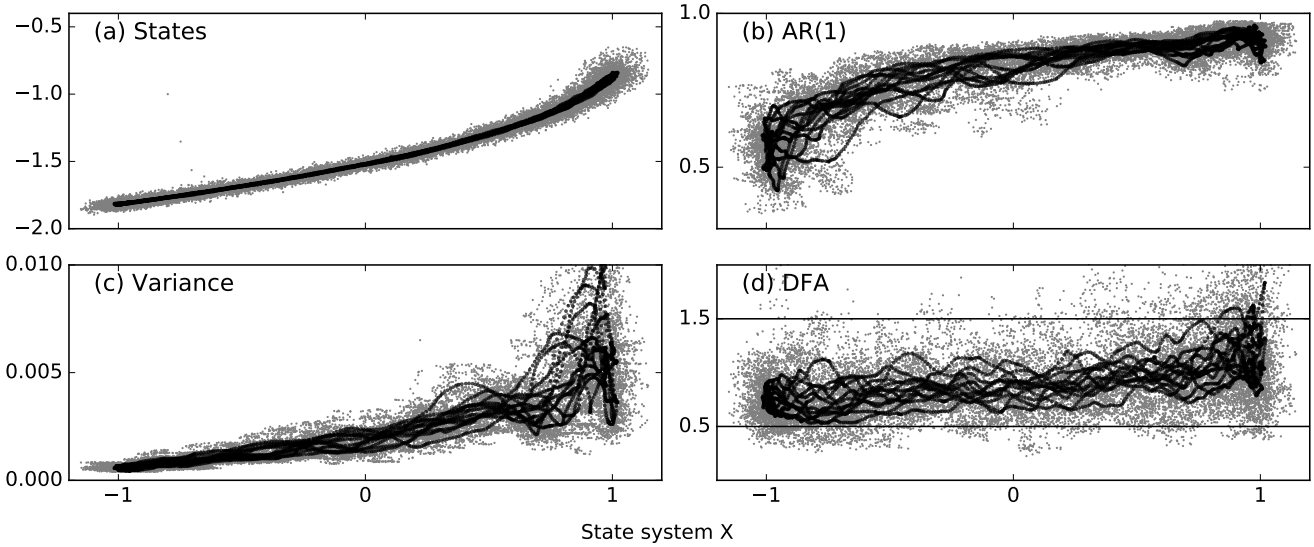

Figure 5. Phase spaces with the windowed statistical indicators of y (vertical) versus windowed mean of the state of x (horizontal) in system 13. From top to bottom, left to right: state, AR(1), variance and DFA scaling exponent (all of the following system y). Grey dots indicate raw data and a running mean with window size 150 is used to get the black dots. Red line in panel (d) indicates linear least squares fit.

Table 1. Parameters used in the ensemble of simulations in the double-fold cascade.

Parameter	Value
$\phi(t)$	0.0012t
$\kappa(x)$	$0.05 + 0.37x$
a_1	-0.5
a_2	0.5
b_1	-0.5
b_2	1
t_{max}	500
Δt	0.5
Noise mean	0
Noise variance	0.1

The results of this ensemble is displayed in Fig. 6. Windows around the bifurcation points are shaded white because this data is misleading when one wants to know what happens before the bifurcation points. We make the distinction between the leading-transitional period (LTP), which is the time series before the first tipping point, and the following-transitional period (FTP), which is the time series between the first tipping point and the second tipping point.

In the LTP, we can clearly see the gradual increasing leading system's variance, AR(1) coefficient and DFA scaling coefficient. These are all evidence of the leading system slowly approaching a bifurcation point, towards which we force it. There is not much evidence of long-range auto-correlations in the time series of the following system, as its variance is low and the DFA scaling exponent remains below 0.5, pointing towards that the detrended fluctuations are statistically white noise. The AR(1) coefficient of the following system does increase just prior to the first tipping, but also stays low.

The detrended cross correlation scaling exponent does give > 0.5 values and gradually increases towards 1.5. This might partly be the direct effect of the simultaneous displacement of the equilibria of both the variables x and y in the pre-transitional period and the direct influence of x on the time derivative of y. However, as the DXA is growing throughout this period, this can also point to long-range cross-correlations strengthening when getting closer towards the bifurcation point of x. We also note that the range of the ensemble is large and therefore not much can be stated to be statistically significant.

The ρ_{DCCA} seems to attain a small positive value (around 0.3) and stays there relatively stable throughout the whole time series. The signal is not so strong, but it seems more robust that the DXA scaling coefficient. One important aspect of the calculation of ρ_{DCCA} as we found by experimentation, is that the trajectory is very sensitive to the segment size s and the moving window size. The moving window determines the amount of data that is available to find long-range correlations, and the segment size has a strong impact on the accuracy of the fits and therefore the segmented fluctuations. As in this analysis, we need a temporal evolution of the statistical indicators, we need moving windows and we thus encounter this problem. As these indicators (DXA and ρ_{DCCA}) have been applied successfully in simpler systems (Zebende, 2011; Podnobik and Stanley, 2007; Zhang et al., 2001; Zhou, 2008), more research on the sensitivity of the indicators with respect to the segment size and moving window

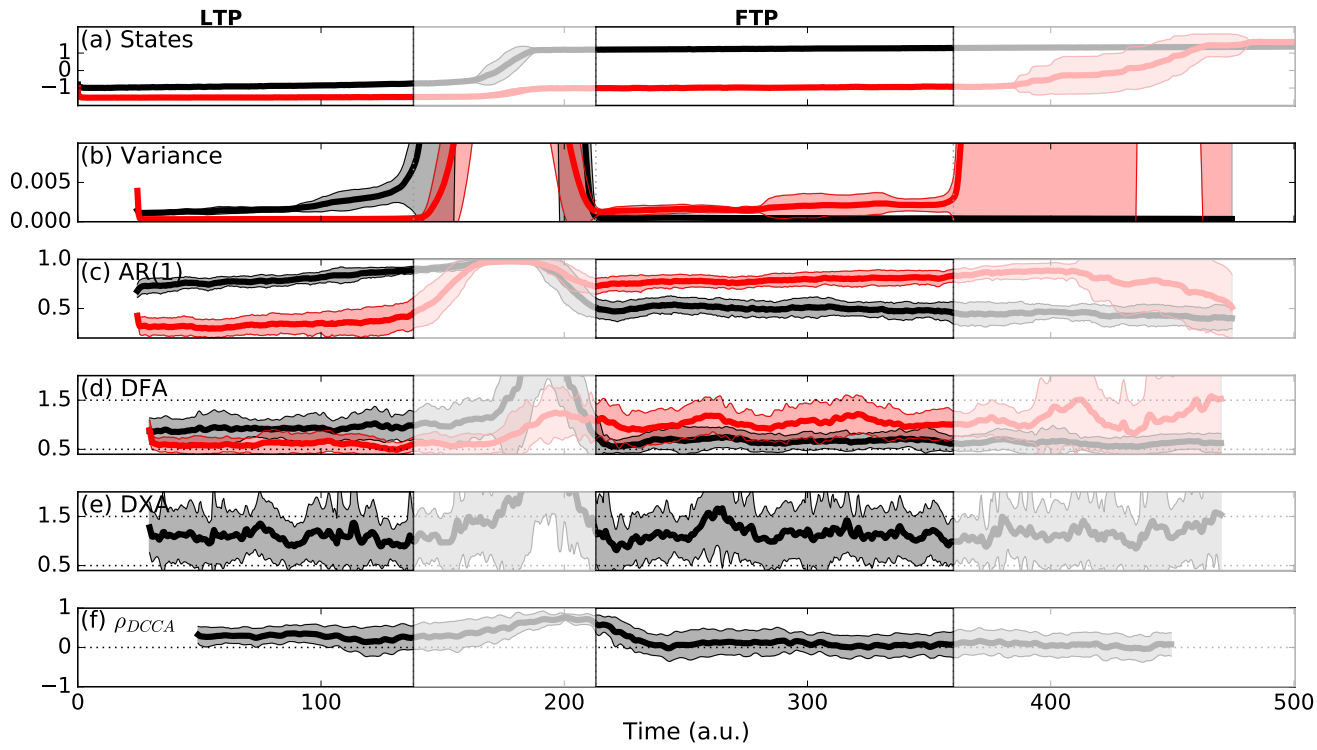

Figure 6. Ensemble simulations with double-fold cascading tipping events, showing (a) states of x (black) and y (red), (b) variance of x (black) and y (red), (c) autoregressive coefficient at lag 1 of x (black) and y (red), (d) detrended fluctuation analysis scaling exponent of x (black) and y (red), (e) detrended cross-correlation analysis scaling exponent and (f) detrended cross-correlation coefficient by Zebende (2011). White-shaded areas indicate windows around the bifurcation points.

size will probably provide more interesting and significant results.

During the FTP, the variance, AR(1) and DFA of the leading system are strongly reduced, but the gradual increasing of the following system's variance, AR(1) coefficient and DFA scaling coefficient are definitely visible, pointing towards the approaching of a bifurcation in the following system. Also notable is the contrast in the DFA of the following system between before and after the tipping of x. The DFA of y went from a white-noise regime (around 0.5) before the tipping of x towards a regime where the detrended fluctuations point towards long-range auto-correlations after the tipping of x (1-1.5). This illustrates the relation between the leading system's state and the following system's DFA scaling exponent, as discussed earlier using system of equations 13.

The DXA remains relatively high, but overall no structural development can be seen in this graph. The ρ_{DCCA} exhibits the same behavior as in the LTP, probably for the reasons already mentioned.

3.3.2 Fold-Hopf cascading tipping

Many statistical indicators have been applied on fold bifurcations specifically, because these transitions show a clear sign of critical slowing down and increased autocorrelation due to the irreversibility and process of going from one equilibrium towards another. A Hopf bifurcation has a different nature with respect to the slowing down, as there is often no hysteresis effect. As there are many critical transitions in climate concerned with Hopf bifurcations (Drijfhout et al., 2015), we will now consider the fold-Hopf cascade in the light of the statistical indicators described before. For this, we use the following stochastic dynamical system:

$$\begin{cases} \dfrac{dx}{dt} = a_1 x^3 + a_2 x + \phi + \zeta_x \\ \dfrac{dy}{dt} = b_1 z + b_2(\kappa(x) - (y^2 + z^2))y + \zeta_y \\ \dfrac{dz}{dt} = c_1 y + c_2(\kappa(x) - (y^2 + z^2))z + \zeta_z \end{cases} \tag{15}$$

where z is the leading system, and (x, y) form the following system, a_i, b_i, c_i are constant parameters, ϕ a forcing term (which we can slowly force in time) and $\kappa(x)$ a coupling term. Noise is added by the terms ζ_x, ζ_y and ζ_z. We simulate an ensemble of 10 runs with the parameter setting as displayed in Tab. 2 and initial conditions $(x_0, y_0, z_0) = (-0.5, 1, -1)$.

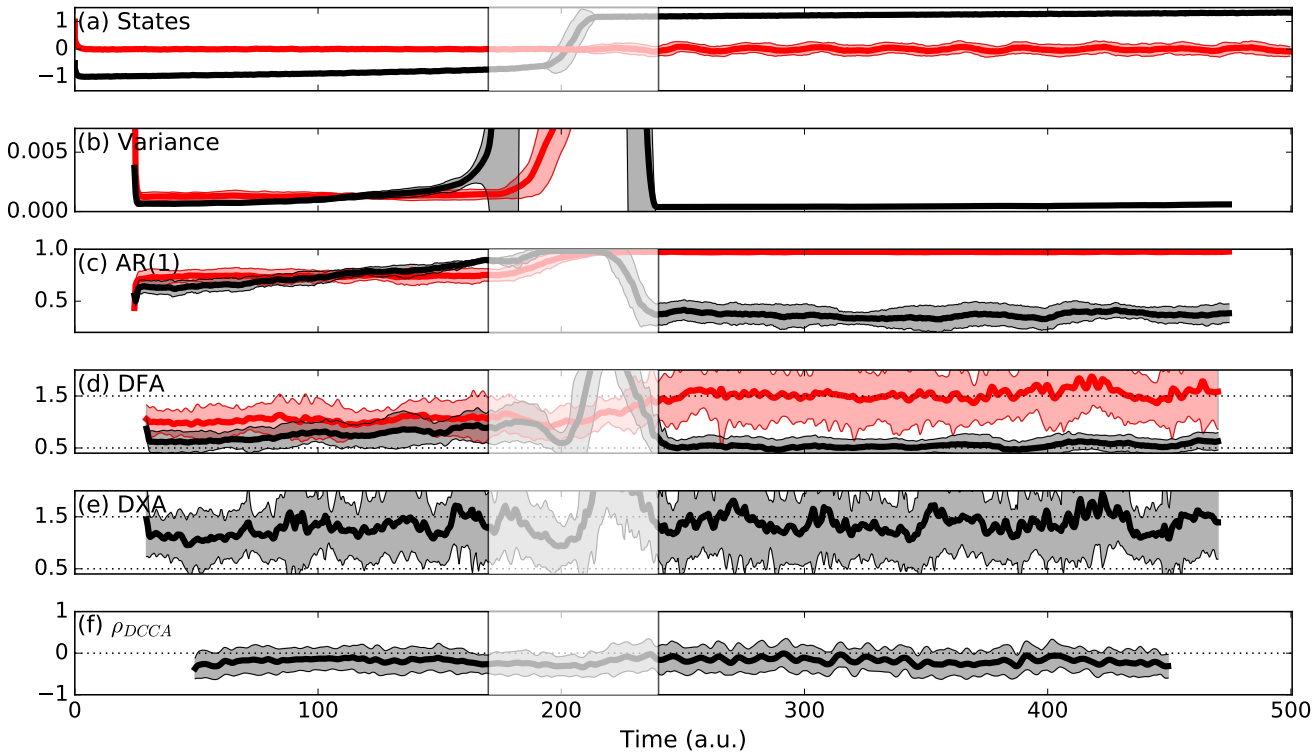

Figure 7. As in Fig. 6, but for the fold-Hopf cascade.

Table 2. Parameters used in the ensemble of simulations in the fold-Hopf cascade.

Parameter	Value
$\phi(t)$	0.002t
$\kappa(x)$	$-0.2+0.3x$
a_1	-1
a_2	1
b_1	0.1
b_2	1
c_1	-0.5
c_2	1
t_{max}	500
Δt	0.5
Noise mean	0
Noise variance	0.1

The results of the ensemble are shown in Fig. 7. Here, we do not make the distinction between the LTP and the FTP, because in contrast to the double-fold cascade, the following system undergoes a critical transition that is easily reversed and that the system either is oscillating, or is stationary. Noise directly starts the oscillation if it is possible, completely removing the FTP. At the start of the time series, the following system is quickly drawn towards the equilibrium state $(x,y)=(0,0)$ and the leading system is fit in the negative equilibrium. During the period towards the bifurcation point, the variance, AR(1) coefficient and DFA of the leading system z gradually increases, as is expected as we force the system towards its bifurcation point.

The DFA and AR(1) of the following system after the bifurcation are in strong contrast with before the bifurcation point, probably due to the autoregressive nature of the oscillation. The relation between the leading system's state and the following system's DFA scaling exponent is also confirmed in this case. The DXA sharply increased just prior to the critical transition, but throughout the whole time series, retains relatively high values. The reason behind this might be found in the low level of noise that is taken, or other simulation-specific parameters. It could also be that it is because the following system on average has a high, weakly varying DFA scaling exponent on itself, which in turn might affect the height and variability in the cross-correlation. The ρ_{DCCA} coefficient remains positive and low, just like in the double-fold case. Again, this can have to do with the choice of window and segment sizes. More research is needed on to relate this variable to cascading tipping events.

4 Application 1: Meridional overturning and ENSO

In this section, the theory of cascading tipping will be applied on the relation between the Atlantic Meridional Overturning Circulation (AMOC) and El-Niño Southern Oscillation

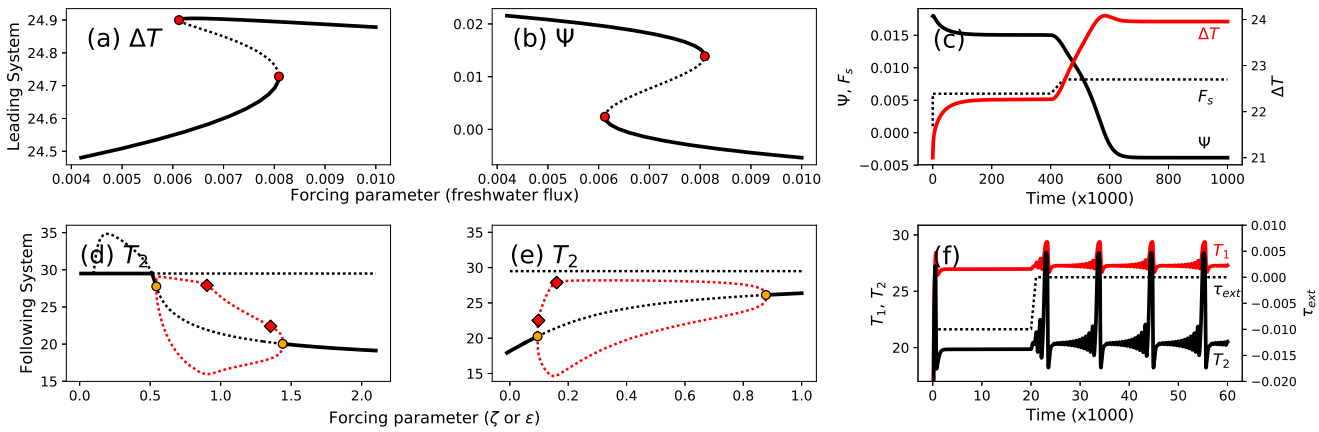

Figure 8. Bifurcation diagrams and forward runs of the Stommel (top) and Timmermann-2003 (bottom) models. In the bifurcation diagrams (left and mid), stable stationary equilibria (black solid), unstable equilibria (black dashed) and oscillatory equilibria (amplitudes in red) are represented, together with fold (red dots), Hopf (orange dots) and period-doubling (red diamonds) bifurcation points. In the forward runs on the right side, the black dashed lines indicate the (ramp function-) forcing and solid lines indicate important variables from the models, specified in the figure itself.

(ENSO). This will be done by building a conceptual model and analyzing the simulations and bifurcation diagrams of the systems, followed by the usage of complex model data from the ESSENCE project.

The overturning circulation has multiple equilibria (Dijkstra and Weijer, 2003; Stommel, 1961) and currently has the potential to tip from a thermohaline (northern and southern sinking) towards a southern sinking state. There are two mechanisms connecting the AMOC to ENSO. The first mechanism is concerned with oceanic waves. A colder North Atlantic creates density anomalies that trigger oceanic Kelvin waves to propagate southward (along the American coast) across the equator. In West Africa, this energy radiates as Rossby waves towards the north and south, which induces Kelvin waves to move along the tip of south Africa into the Indian ocean, that eventually reach the Pacific. Consequently, the eastern equatorial Pacific thermocline deepens on a timescale of decades. This deepening has a weakening effect on the amplitude of ENSO (Timmermann et al., 2005).

The second mechanism is concerned with the trade winds. Cooling in the northern tropical Atlantic (due to MOC weakening) induces anti-cyclonic atmospheric circulation (Xie et al., 2007) that intensifies the northerly trade winds over the northeastern tropical Pacific. This leads to a southward displacement of the Pacific ITCZ (Zhang and Delworth, 2005) and this generates a meridional SST anomaly due to anomalous heat transport and the wind-evaporation SST feedback in the Pacific. Also, Dong and Sutton (2007) found an atmospheric coupling through Rossby waves sent into the northeast tropical Pacific. The result of the wind stress as coupling between the two systems is an intensification of ENSO and this mechanism is argued to be stronger than the coupling through oceanic waves (Timmermann et al., 2005).

4.1 Model details

To apply the theory of cascading tipping to this case, a conceptual model is needed where we can explicitly calculate the bifurcation diagram. We will discuss the leading and following system separately below.

4.1.1 Leading system - Meridional Overturning

The model we use for the meridional overturning is the classic Stommel box model from Stommel (1961), consisting of a polar (subscript p) and an equatorial box (subscript e), both with a temperature T and salinity S. The state variables are then defined as $\Delta T = T_e - T_p$ and $\Delta S = S_e - S_p$. The time evolution of these variables is as follows:

$$\begin{cases} \dfrac{d\Delta T}{dt} = & -\dfrac{1}{t_r}(\Delta T - \theta_0) - Q(\Delta\rho)\Delta T \\ \dfrac{d\Delta S}{dt} = & \dfrac{F_s}{H}S_0 - Q(\Delta\rho)\Delta S \end{cases} \tag{16}$$

where the first terms in both equations refer to temperature and salinity relaxation towards a certain mean state, and the second term refers to density-driven meridional transport. Specifically, t_r is the surface temperature restoring time scale, θ_0 is the equator-to-pole atmospheric temperature difference, $Q(\Delta\rho)$ is the transport function, which is calculated from a diffusion time scale and the meridional density gradient $\Delta\rho$, S_0 is a reference salinity, and H is the ocean depth. The parameter F_s is the freshwater flux, which can be used as a bifurcation parameter. We also define a flow function:

$$\begin{aligned} \Psi &:= \gamma\Delta\rho/\rho_0 \\ &= \gamma(\alpha_T\Delta T - \alpha_s\Delta S) \end{aligned}$$

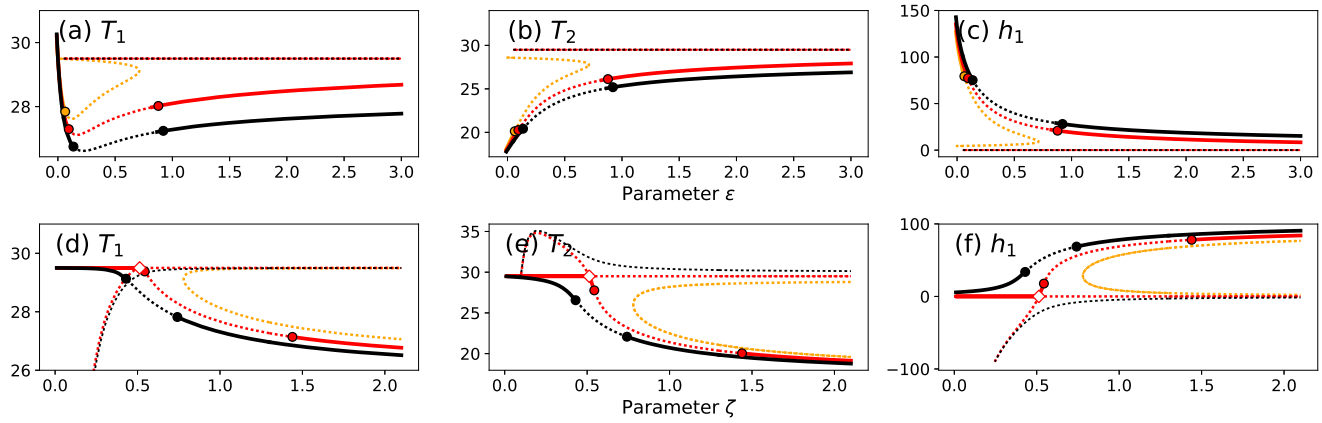

Figure 9. Top: equilibrium diagrams w.r.t. ϵ of T_1 (left), T_2 (center) and h_1 (right) for different values of τ_{ext}: -0.01 (black), 0 (red) and 0.01 (orange). Dots indicate Hopf bifurcations and white diamonds indicate branch points. We use $\zeta = 1.3$ here. Bottom: same as top, but for variable ζ ($\epsilon = 0.1$).

which represents the MOC, with $\gamma > 0$ a certain flow parameter, ρ_0 a reference density and α_T, α_S the thermal and haline expansion coefficients.

4.1.2 Following system - El-Niño Southern Oscillation

Concerning the El-Niño Southern Oscillation, bursting behavior and various oscillations within this phenomenon need to be captured within the conceptual model. Timmermann et al. (2003) investigated this and came up with a model with a state vector consisting of the temperature of the western Pacific T_1, the temperature of the eastern Pacific T_2 and the thermocline depth of the western Pacific h_1. Their model finds its basis in the Zebiak and Cane (1987) ENSO model, with a two-strip and two-box approximation, and a shallow-water model for the upper ocean with a fixed mixed layer depth:

$$\begin{cases} \dfrac{dT_1}{dt} = & -\alpha(T_1 - T_r) - \dfrac{u(T_2 - T_1)}{L/2} \\ \dfrac{dT_2}{dt} = & -\alpha(T_2 - T_r) - \dfrac{w(T_2 - T_{sub})}{H_m} \end{cases} \tag{17}$$

with $1/\alpha$ a typical thermal damping timescale, T_{sub} the temperature below the mixed layer, H_m and L the depths of the mixed layer and basin width, respectively, w upwelling velocity and u atmospheric zonal surface wind being linear to wind stress: $u/(L/2) = \epsilon\beta\tau$ and $w/H_m = -\zeta\beta\tau$. The parameters ϵ and β refer to the strength of zonal and vertical advection (bifurcation parameters). Wind stress τ is expressed as (neglecting annual cycle and noise):

$$\tau = \frac{\mu(T_1 - T_2)}{\beta} \tag{18}$$

with μ/β parameters that control the influence of the zonal temperature gradient on the wind stress, set to be 0.02 Pa·K^{-1}. The subsurface temperature T_{sub} is parametrized as

$$T_{sub} = T_r - \frac{T_r - T_{r0}}{2}\left[1 - \frac{\tanh(H + h_2 - z_0)}{h*}\right] \tag{19}$$

with h_2 the east equatorial Pacific thermocline depth (calculated as deviation from a reference depth H), z_0 the depth for which w becomes its characteristic value and $h*$ the sharpness of the thermocline. The thermocline depths are calculated as follows:

$$\begin{cases} h_2 = & h_1 + bL\tau \\ \dfrac{dh_1}{dt} = & r(-h_1 - \dfrac{bL\tau}{2}) \end{cases} \tag{20}$$

where b the efficiency of wind stress τ to drive the thermocline tilt. For further details and parameter values, we refer to Timmermann et al. (2003).

4.2 Results

We start with running the dimensional Stommel and Timmermann models separately. The dimensional Stommel bifurcation diagrams are shown in Fig. 8a and b, clearly showing a saddle-node structure. It can already be seen that for some values of the freshwater flux F_s, the system has multiple equilibria, and for other values, only one equilibrium remains. This means that when we are in the high-Ψ branch and F_s is large enough, the system will critically transit towards the low-Ψ branch. An example simulation of such an event is shown in Fig. 8c.

The bifurcation diagrams of the Timmermann model for parameters zonal advection ϵ and vertical advection ζ are shown in Fig. 8d and e. There are Hopf and period-doubling bifurcations close to the realistic values of of $(\epsilon, \zeta) \approx (0.05-0.24, 1.3)$ (Timmermann et al., 2003). This means that under the right forcing, this system can undergo drastic change, attaining or losing periodic behavior (Hopf) or changing the

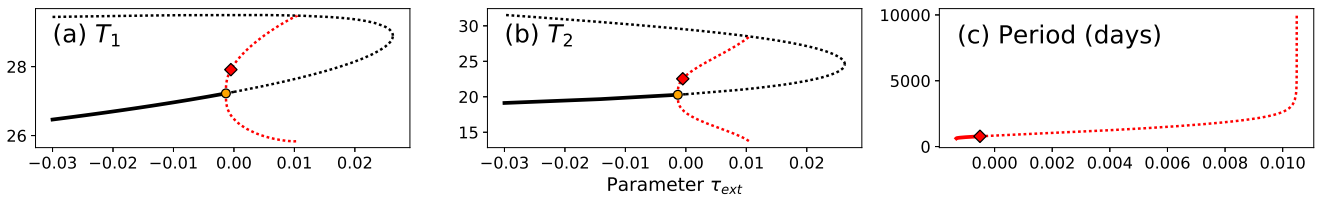

Figure 10. Bifurcation diagrams of the following system depending on the coupling parameter τ_{ext}, for the standard values of $\epsilon = 0.1$ and $\zeta = 1.3$.

intensity of this behavior (period-doubling). An example of a run where such a forcing is applied after a while can be seen in Fig. 8f, where a Hopf bifurcation is crossed.

As we know from literature (described above), the coupling of the two systems is mainly through influence on the wind stress. In Timmermann et al. (2003), the wind stress is only dependent on zonal SST gradients in the Pacific. We will now add a term τ_{ext} that is dependent on meridional temperature gradients in the Atlantic ΔT:

$$\tau = \tau_{ext}(\Delta T) + \frac{\mu}{\beta}(T_2 - T_1) \tag{21}$$

with a negative relation between τ_{ext} and Atlantic meridional SST gradient ΔT as we know from literature described above (stronger positive ΔT results in stronger easterlies, thus negative τ_{ext}). We do note that both the total Pacific wind stress τ and specifically τ_{ext} should always be negative. The total wind stress is negative because this area (at low altitude) is strictly dominated by easterly winds, and τ_{ext} is negative because through the meridional temperature gradient, it reflects the influence of the zonal mean Hadley cell on the equatorial Pacific. Physically, the Hadley cell only induces negative zonal wind stress in this region.

The equilibrium diagram of the Timmermann-2003 model with τ_{ext} as bifurcation parameter is shown in Fig. 10. In the lower (stable) branch, a Hopf and a period doubling bifurcation can be recognized. This structure of the diagram is quite consistent for different values of ζ and ϵ. The parameter τ_{ext} merely repositions the Hopf and period-doubling bifurcation points. The period of the oscillation varies with τ_{ext} as can be seen in Fig. 10c. This means that τ_{ext} can modulate whether the system is in an oscillatory or stationary state and what the intensity is of the oscillatory state. However, the range for which τ_{ext} is realistic is of course limited; the total wind stress τ and τ_{ext} are negative (as described above). For completeness, also positive values of τ_{ext} are shown in Fig. 10. Ocean-atmosphere coupled complex model runs with different Atlantic overturning states might prove useful to quantify the relation between τ_{ext} and ΔT more specifically.

Varying τ_{ext} also changes the equilibrium diagrams with respect to ζ and ϵ. Figure 9 shows the equilibrium diagrams of all three state variables for different values of τ_{ext}, with respect to ζ and ϵ. It is visible that (as already seen in Fig. 10a) in all cases of τ_{ext}, the parameter set $(\epsilon, \zeta) = (0.1, 1.3)$ allows for both a stable oscillatory equilibrium and an unstable stationary solution. The latter involves the state where $T_1 = T_2 = T_R$ (relaxation temperature, 29.5) and $h_1 = \tau_{ext} = 0$, with much higher values of T_2 than usual and slightly higher values of T_1 than in stable equilibria. It is to this state towards which the oscillation of El-Niño events can excite to for a short period of time. This unstable state is visible as a high-T, low-h_1 horizontal dashed line in all panels of Fig. 10. When decreasing τ_{ext}, the difference between the states rise, but the Hopf bifurcation points in (ϵ, ζ) space change, too, meaning that with the parametrization of (0.1,1.3), our state moves towards the edge of the oscillating domain, decreasing the intensity of the oscillation and lowering its period. When τ_{ext} is increasing, the opposite happens. This indicates that El-Niño intensifies when τ_{ext} is increased, also for realistic values.

Using τ_{ext} to couple the Stommel and Timmermann, we ran simulations with $\Delta t = 0.1$, the Runge-Kutta fourth order integration method, a freshwater forcing F_s in the form of a ramp function and a coupling of τ_{ext} expressed in terms of ΔT. The exact quantification of this modulates which effect the collapse of the overturning has on ENSO. The results of the simulation are shown in Fig. 11. In the first case (upper panel), the collapse of the overturning leads to the crossing of a period-doubling bifurcation point in the following system, and a clear intensification of the oscillation is visible. In the latter case (lower panel), a Hopf bifurcation is crossed in the following system, starting an oscillation. In both cases we can conclude that the behavior of ENSO changes drastically if the AMOC collapses. This is an illustrative example of a type 2 (fold-Hopf) cascading tipping event.

4.3 Verification with complex model output

To gain insight in the evolution of ENSO in the case of a collapse of the overturning, we need more complex models that include such a behavior of the overturning. ESSENCE (Ensemble SimulationS of Extreme weather events under Nonlinear Climate changE) is a project where several experiments have been done with the ECHAM5/MPI-OM coupled climate model, including hosing experiments. The temporal resolution used is monthly data between 1950 and 2100. The

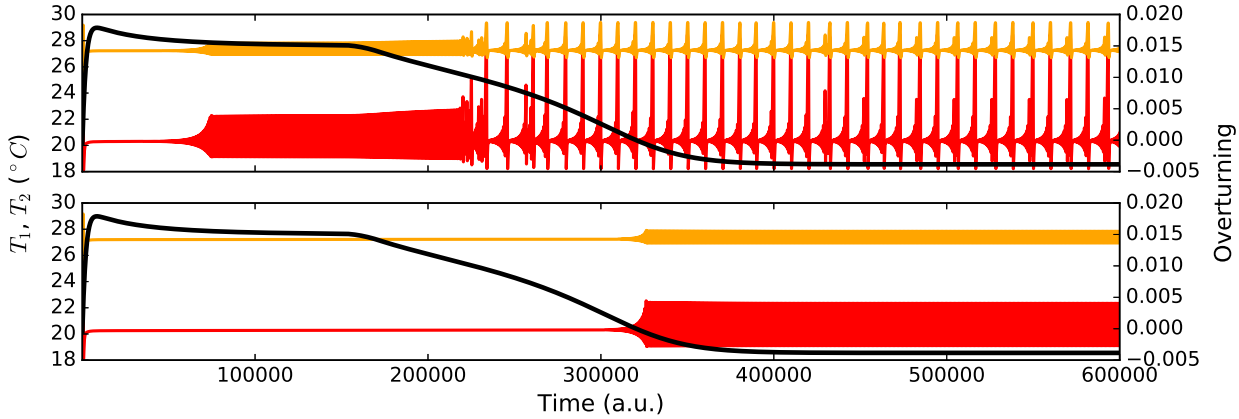

Figure 11. Simulation run of the coupled Stommel-Timmermann model for different model configurations, where the collapse of the overturning flow function (black) leads to the crossing of a Hopf bifurcation (top) or period-doubling bifurcation (bottom) in ENSO. Following variables are western tropical Pacific temperature (orange), eastern tropical Pacific temperature (red) and eastern tropical Pacific thermocline (yellow).

spatial fields are on a curvilinear grid, with 40 vertical levels in the ocean. We define the overturning strength as the maximum Atlantic stream function at 35°N and ENSO intensity as the El-Niño 3.4 index, which is the average SST over 170°-120°W and 5°S - 5°N.

Two ensembles of the ESSENCE project have been used in this section; the HOSING-1 experiment ensemble and the 'standard' SRES-A1b ensemble. Five runs of each ensemble are taken, specifically runs 041-045 of the HOSING-1 and runs 021-025 of the SRES-A1b ensemble. The HOSING-1 ensemble contains a hosing experiment in the classical way, following the procedure of Jungclaus et al. (2006). One Sv of fresh water is added around Greenland from the end of year 2000 onwards.

The results for the evolution of the overturning are shown in Fig. 12. It is clearly visible that the hosing experiment destabilizes the overturning. The Atlantic stream function at 35°N decreases by approximately 85%. The results for the evolution of ENSO is shown in Fig. 12.

Table 3 compares the period before and after 2001, which is the year at which the hosing starts. We use deseasonalised data because we are interested in interannual variability, not in seasonal variability, as El-Niño is associated with these timescales. We use the non-anomaly statistics, as this gives us information about the differences in the mean. We do note that we only use five runs per ensemble, which makes the uncertainty not statistically robust. We only state it in Tab. 3 to give an idea of the range of the variables among the different runs.

It is visible in Tab. 3 that the variability of the El-Niño 3.4 SST increases (bold numbers) if we compare the periods of 1950-2000 and 2001-2100. This increased variability is visible in both the standard and the HOSING-1 runs. However, the variability is increased much stronger in the HOSING-1 experiment, indicating that the collapse of the overturning

Table 3. ENSO 3.4 SST statistics (of deseasonalised data) for the different ensembles. The uncertainty stated is the standard deviation among the five runs within the ensemble.

Time period	Ensemble	Variable	Value
1950-2000	Standard SRES-A1b	Mean	25.86 $\pm$ 0.046
	Standard SRES-A1b	Variance	**1.705** $\pm$ 0.447
2001-2100	Standard SRES-A1b	Mean	27.51 $\pm$ 0.032
	Standard SRES-A1b	Variance	**2.581** $\pm$ 0.112
2001-2100	HOSING-1	Mean	27.27 $\pm$ 0.053
	HOSING-1	Variance	**3.21** $\pm$ 0.42

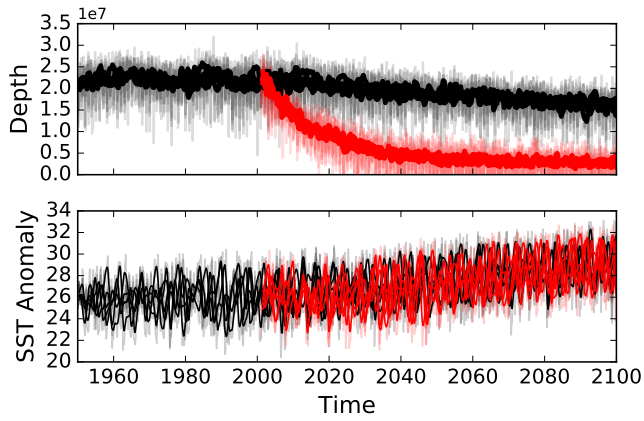

Figure 12. Top: Evolution of the five standard SRES-A1b runs (blue) and five HOSING-1 runs (red) in terms of the overturning. Bottom: ENSO 3.4 SST of the standard SRES-A1b ensemble (blue) and the HOSING-1 ensemble (red). Shaded thin lines indicate monthly means, thick lines indicate the deseasonalised values.

indeed has an amplifying effect on ENSO. The large difference between the standard and hosing runs suggests that the ENSO 3.4 index underwent stochastic critical transition in the hosing experiment, as a consequence of the collapse of the overturning. Further research is needed whether this is true.

5 Application 2: Meridional overturning and land ice

At the Eocene-Oligocene transition, marine records of δ^{18}O indicate an abrupt increase of 1.2-1.5‰. Within this transition, a two-step signal can be recognized with two 40-kyr steps, separated by a 200-kyr plateau. A persisting maximum is attained for 400 kyr and is stepwise decreased and stabilized to a value still about 1‰ higher than before the transition (Coxall et al., 2005). The two steps are attributed to a deep-sea temperature drop followed by the (slower) growth of the Antarctic Ice Sheet (AIS). The deep-sea temperature drop can have to do with a switch in overturning state, as investigated in Tigchelaar et al. (2011). The cause of the ice sheet formation is still a matter of debate. A first hypothesis could be the opening of ocean gateways like the Drake Passage and Tasmanian Passage, which allowed for the arising of the Antarctic Circumpolar Current. This current strongly cools Southern Ocean SSTs and might facilitate the origin of the Antarctic Ice Sheet. However, timing of these gateways is proven to be problematic (Coxall and Pearson, 2007), there is not much evidence for a strong ACC before the mid-Miocene (16.0–11.6 Ma) (Coxall and Pearson, 2007) and to attain significantly decreased Antarctic continental temperatures, the ocean heat transport would have decreased enormously (Huber and Nof, 2006).

Another explanation for the onset of the Antarctic Ice Sheet formation is found in the reaching of a certain CO_2 threshold, that would induce snow/ice-albedo and ice-sheet height/mass balance feedbacks to initiate ice growth (Pearson et al., 2009; Coxall et al., 2005; DeConto and Pollard, 2003). This might have been aided by certain orbital settings at that time (DeConto and Pollard, 2003; Coxall et al., 2005; Coxall and Pearson, 2007).

We know that the overturning circulation has an impact on atmospheric CO_2 mixing ratios due to the fact that in a SPP state, the stronger upwelling in the northern hemisphere brings up more CO_2, while in a TH state this is more suppressed. This rises the question to which extent the switch in overturning circulation impacts the atmospheric CO_2 and therefore indirectly drive the growth of the AIS (a second tipping point). If this impact is strong enough, a cascading tipping event may occur. This section is not intended to propose this as the mechanism driving the EOT, but describes an interesting case study in the light of potential cascading tipping events, specifically the type 1: double-fold cascading tipping.

5.1 Model details

To conceptually analyze such an event, we use a model as proposed in Gildor and Tziperman (2000, 2001) and (Gildor et al., 2002) and adapted in Tigchelaar et al. (2011). The model consists of four latitudonal boxes, has two layers in the ocean (8 ocean boxes) and one layer in the atmosphere (4 atmosphere boxes). The boundaries of the boxes represent the South Pole, 45°S, the equator, 45°N and the North Pole. Its equations consists of simple frictional momentum balances, which are hydrostatic and mass conserving. Temperature and salinity are determined by advection, diffusion and radiative fluxes (for which the albedo is a combined number based on surface composition within the box). Precipitation is calculated from the convergence of moisture fluxes. The overturning (leading system) is buoyancy driven, which means that it can be forced with a density perturbation. The land ice model (following system) is based on ice sheet growth (directly proportional to precipitation) and a constant ablation term. The resulting ice sheet is zonally symmetric and has perfect plasticity. A maximum amount of ice volume is defined for the Antarctic (south hemisphere polar box) ice sheet to be $2.57 \cdot 10^{16}$ m^3, to prevent growth beyond realistic volumes (Tigchelaar et al., 2011). There is no sea ice in this model. Computations of δ^{18}O are proposed in Tigchelaar et al. (2011). Because we want to couple a collapse of the overturning to land ice, we need to include the chemistry module, which resolves advection, diffusion and chemical interaction of three chemicals: CO_2, alkalinity and phosphate (PO_4). For an overview of the equations and parameter settings, we refer to Gildor and Tziperman (2001) and Gildor et al. (2002). Because albedo is calculated as a composition of ice, land and ocean partitions within each box, albedo-ice feedback is included in this model and therefore CO_2 can affect ice equilibria.

Tigchelaar et al. (2011) already describes several stable states in this model's overturning circulation: the southern sinking state (SPP), the northern sinking state (NPP) and a state at which there is sinking at both poles (thermohaline, TH) are found to be stable depending on the parameter settings. The SPP and TH state are illustrated in Fig. 13. Southern hemispheric land ice has two stable equilibria in the model (depending on the parameter settings): no ice, and the fully ice-covering maximum volume.

5.2 Results

The example of the Eocene-Oligocene transition involves the transition of the overturning circulation from a SPP state towards a TH state and an active geochemistry. The active chemistry resulted in a high CO_2 concentration (1500 ppm) for the standard parameter settings, making ice impossible to grow. The vertical diffusion coefficient K_v in the ocean boxes can be adapted (within reason) to alter this. If K_v is low, less CO_2 is brought upward (and into the at-

mosphere), resulting in lower atmospheric CO_2 concentrations. The southern hemispheric melt temperature T_{melt} can be used to tune at which atmospheric CO_2 concentration ice starts to grow.

Both parameters K_v and T_{melt} need to be tuned such that the resulting case is most realistic. This means that K_v should be such that CO_2 is brought down far enough (down to roughly 800 ppm) by a change in overturning state. This resulted in $K_v = 1 \cdot 10^{-9}\ \mathrm{m^2 s^{-1}}$. The T_{melt} should be such that ice feedbacks are possible at the resulting CO_2 levels, but that ice does not switch in regime merely because of the temperature change due to the overturning switch. This resulted in a melt temperature T_{melt} of 274 K. A spin-up run of 120,000 years was needed to let the system come into an equilibrium SPP state. Then, a 10,000 years run is done to adapt to an active geochemistry and the renewed values of K_v and T_{melt}. After this, a 100 y-long high density ($1030\,\mathrm{kg\,m^{-3}}$) perturbation is applied in the upper northern hemispheric polar ocean box. This forces a transition of the overturning from the SPP state towards a TH state and is shown in Fig. 14.

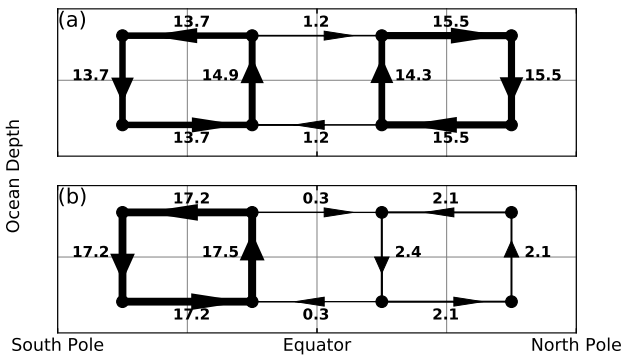

Figure 13. Oceanic flow in a typical thermohaline (TH) state (a) and southern sinking (SPP) state (b). Numbers and arrow thickness indicate flow vectors from the simulation shown in Fig. 14, far before and after the tipping.

Figures 13 and 14a clearly shows the transition of a SPP state (where vertical transport in the northern hemisphere is almost zero) towards a TH state in this simulation, and the fast reaction of the system to the density perturbation. We see that directly after the transition, the system slowly adapts to the new state, with slightly decreasing ocean and atmospheric temperatures and rapidly decreasing CO_2 (from about 1500 ppm to 850 ppm). When CO_2 reaches about 900 ppm, southern hemisphere polar ice starts to grow. The decreased CO_2 decreases atmospheric and oceanic temperatures in almost all boxes, although northern hemispheric polar temperatures effectively rose with the overturning transition because there is now downwelling (of relatively warm surface water) in this box instead of upwelling (of cold deep water).

This is an example of a cascading tipping event, because the ice starts growing because of a changed equilibrium regime modulated by CO_2, rather than simply decreased atmospheric temperatures.

5.3 Two-step signal in δ^{18}O

Looking at the δ^{18}O graph in Fig. 14c, one can see a strong increase directly after the transition in the overturning circulation, prior to ice formation (between t =10 and 17 kyr), indicating the effect of an overturning transition on deep sea temperatures. After this temperature effect is roughly settled, ice starts forming and slowly increases the δ^{18}O to a much higher value. It takes about 90 kyr to grow to its maximum size. In this model, a lag is found between overturning transition and the ice formation onset, with a size of 7 kyr. The fact that this is so short makes the temperature and ice effects on the δ^{18}O overlap, removing a potential plateau in between. As mentioned before, in the actual EOT, this plateau is about 200 kyr and the separate transitions 40 kyr, making the effects seen in this model incomparable with the actual case. A problem with these simulations is that we did not include precise orbital forcing, which may delay the ice formation dramatically. For example, it could be that the CO_2 remain just above the critical threshold after the overturning switch, but crosses the threshold much later due to orbital forcing. Still, the model shows an interesting mechanism that could drive a type 1 cascading tipping in climate science.

6 Summary and Conclusions

In this paper, we introduce the concept of cascading tipping. It is defined as the event of a critical transition in a first, leading system, altering background conditions (that is, the regime in the equilibrium diagram) such that another critical transition in a second, following system occurs.

We created a mathematical framework around this concept, where we used back-to-back saddle-node and Hopf bifurcations to make simulations of critical transitions. Exact positions of these bifurcations in terms of parameter thresholds are investigated and explicitly expressed. General forms of dynamical systems are formulated of four deterministic cascading tipping types, including the (1) double-fold cascade, the (2) fold-Hopf cascade, the (3) Hopf-fold cascade and the (4) double-Hopf cascade. We found that the following system's bifurcation structures can be expressed in terms of the forcing term in the leading system and that we can this way predict the behavior of the following system when the coupling is known. In the case of stochastic systems, we discussed the effect on the PDF and flickering effects, allowing for more subtle critical transitions.

Subsequently, we discussed statistical indicators and analysis tools for critical transitions. Starting off with the general theory of critical slowing down, we continued with degener-

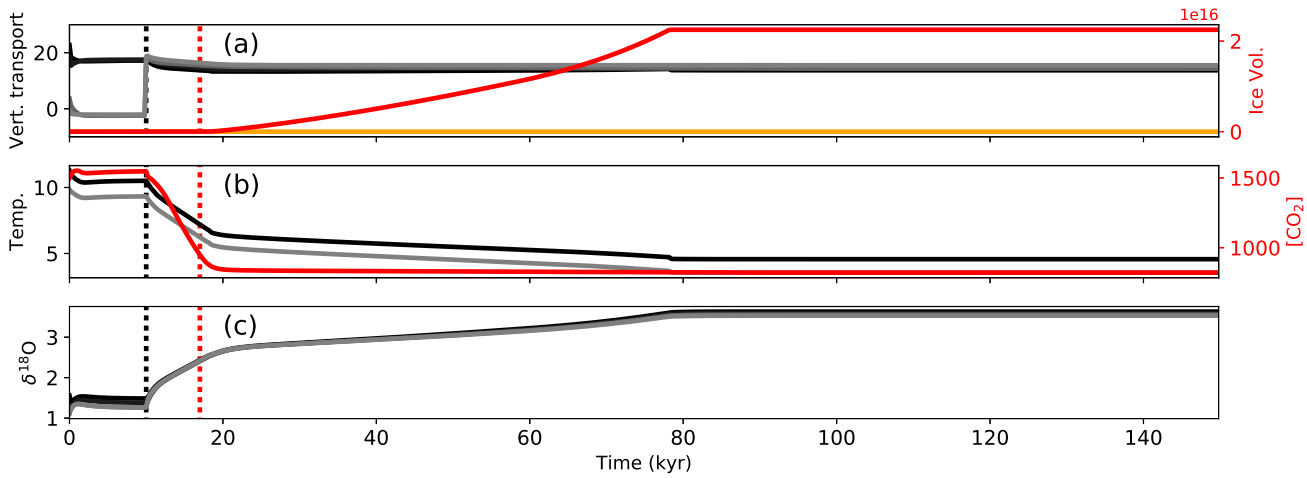

Figure 14. Simulation run of the Gildor-Tziperman model, showing a cascading tipping event; (a) Vertical transport (grey shades from North Pole to South Pole) with ice volume (red: SH, orange: NH), (b) atmospheric (grey) and upper ocean (black) temperature of the SH polar box with CO_2 mixing ratio (red), (c) δ^{18}O isotopic ratio (grey shades from north polar box to south polar box). Vertical dashed black line indicators the moment of density perturbation (i.e., critical overturning transition). Vertical dashed red line indicates moment at which ice starts to form.

ate fingerprinting and detrended fluctuation analysis (DFA), that present early warnings for single tipping points. Indicators for cascading tipping points are found in detrended cross correlation analysis (DCCA) and a special case of extrapolation using the DFA of the following system. These tools are applied in simulations involving both the double-fold and fold-Hopf cascades. The increased variance, AR(1) and DFA scaling exponent are clearly found in each case of single tipping. The cross-correlation indicators (DCCA and ρ_{DCCA}) did not evolve much throughout the time series (except for very close with respect to the tipping points), which may indicate their invariance with respect to proximity to single tipping points. Some limitations of the presented analysis of these variables have been mentioned. Surprisingly, it turns out to be useful and, in many conceptual cases, possible to retrieve information from the relation between the leading system's state and the following system's DFA to predict cascading tipping events.

The concept of cascading tipping is applied to two climatological cases. The first is concerned with the link between the overturning circulation and ENSO. We modelled this using a coupling between the Stommel (1961) model and an ENSO-model by Timmermann et al. (2003) through a meridional temperature gradient-dependent term in the wind stress of the ENSO-model. Through analysis of the bifurcation diagrams and simulations, cascading tipping events are indeed possible in this case and the results are elaborated on in the light of previous research.

The second application is found in the impact of the overturning on land ice formation, coupled through atmospheric CO_2. This case was inspired by a two-step signal in the δ^{18}O during the Eocene-Oligocene transition, where the switch from a southern sinking (SPP) state to a thermohaline (TH) state was followed by the arising of the Antarctic Ice Sheet. Using a box model by Gildor and Tziperman (2000), we were able to simulate a cascading tipping event as expected from theory, but the timescales and simplicity of the simulations make them incomparable to the actual EOT.

The mathematical framework and discussed simulations and statistical analysis form a basis of this new concept. More research can be done on the various types of cascading tipping and also on the creation of well-suited indicators and early warnings of such events.

The two applications highlight that there are scenarios in which these events occur in climate and therefore highlight the importance of this topic. As by definition, critical transitions involve drastic change and consequences, the coupling between these transitions (be it in the form of cascading tipping) remains a relevant topic. Future research will point out whether these events are likely to happen and whether this effect is also present in other fields than climate science.

Appendix A: Proofs concerning critical thresholds

Lemma 1. *The system x in Eqn. 1 has at maximum one stable equilibrium when $a_1 > 0$.*

Proof. Because Eqn. 1 is a third degree polynomail, we know that it has at maximum three roots (by induction; a linear function has one root and use the mean value theorem) and at minimum one root (intermediate value theorem) for both the cases of $a_1 > 0$ and $a_1 < 0$. Such roots coincide with

equilibria, which are stable if and only if $\dot{x}(x_0+\delta)<0$ and $\dot{x}(x_0-\delta)>0$ for any small $\delta\in\mathbb{R}$. Now assume $a_1>0$.

Further assume that there is only one equilibrium, at $x=x_0$. Then we know that $\dot{x}(-\infty)\to-\infty$, indicating that $\dot{x}(x_0-\delta)<0$ for small arbitrary $\delta\in\mathbb{R}$. This means that x_0 is instable. Say there is a second equilibrium (x_1), in a total of two. The instability for the first equilibrium remains because we can use the exact same reasoning. We also know that because $\dot{x}(+\infty)\to+\infty$, it follows that $\dot{x}(x_1+\delta)>0$, indicating that also this equilibrium is instable. Now, say there are three equilibria. We then know that the first and third are instable because of the same reasoning as above. This leaves only one equilibrium to be potentially stable. □

Lemma 2. *The system x in Eqn. 1 has multiple equilibria if and only if $a_1<0$, $a_2>0$ and $|a_3|<\sqrt{\frac{-4a_1^3a_2^3}{27a_1^4}}$.*

Proof. From Lemma 1 we know that there are no multiple equilibria in system x if $a_1\le 0$. We also know that if $a_1=0$, the system is linear, $\frac{dx}{dt}$ has only one root and does therefore not have multiple equilibria. We conclude that $a_1<0$ is necessary to attain multiple equilibria in $\dot{x}$.

For multiple equilibria to arise, we need a regime in which $\frac{d^2x}{dt^2}>0$, because otherwise the time propagation of x would be monotonously decreasing and having only one root. $\frac{d^2x}{dt^2}>0$ gives $3a_1x^2+a_2>0$, resulting in $|x|>\sqrt{-a_2/(3a_1)}$. Given $a_1<0$ (reasoned above) and $a_2\neq 0$ (otherwise $\frac{d^2x}{dt^2}\le 0$ for all x), this only has real solutions if $a_2>0$. We conclude that $a_2>0$ is then also necessary to enter a domain in which multiple equilibria are possible for x.

Now the question remains whether there are multiple equilibria (that is, roots) in $\frac{dx}{dt}$. For this we need to solve the system $\frac{dx}{dt}==0$. Using a solving algorithm software, the following three solutions for have been found:

$$
\begin{aligned}
x_0 &= \frac{(\sqrt{3}\sqrt{27a_1^4a_3^2+4a_1^3a_2^3}-9a_1^2a_3)^{\frac{1}{3}}}{\sqrt[3]{2}\sqrt[3]{9}a_1} \\
&\quad -\frac{\sqrt[3]{2/3}a_2}{(\sqrt{3}\sqrt{27a_1^4a_3^2+4a_1^3a_2^3}-9a_1^2a_3)^{\frac{1}{3}}} \\
x_1 &= \frac{(1+i\sqrt{3})a_2}{(12\sqrt{3}\sqrt{27a_1^4a_3^2+4a_1^3a_2^3}-108a_1^2a_3)^{\frac{1}{3}}} \\
&\quad -\frac{(1-i\sqrt{3})(\sqrt{3}\sqrt{27a_1^4a_3^2+4a_1^3a_2^3}-9a_1^2a_3)^{\frac{1}{3}}}{\sqrt[3]{144}a_1} \\
x_2 &= \frac{(1-i\sqrt{3})a_2}{\sqrt[3]{12}(\sqrt{3}\sqrt{27a_1^4a_3^2+4a_1^3a_2^3}-9a_1^2a_3)^{\frac{1}{3}}} \\
&\quad -\frac{(1+i\sqrt{3})(\sqrt{3}\sqrt{27a_1^4a_3^2+4a_1^3a_2^3}-9a_1^2a_3)^{\frac{1}{3}}}{\sqrt[3]{144}a_1}
\end{aligned}
$$

The system has multiple equilibria if and only if all roots have non-equal real part (given $a_1<0$ and $a_2>0$). We therefore need $27a_1^4a_3^2+4a_1^3a_2^3>0$, or $|a_3|<\sqrt{\frac{-4a_1^3a_2^3}{27a_1^4}}$. □

Lemma 3. *The system x and y in Eqn. 2 reaches a stable periodic solution when coming from a stable stationary equilibrium if and only if $a_1b_1<0$ and $a_2a_3+b_2b_3=0$.*

Proof. From bifurcation theory we know the equations for x and y in Eqn.2 to be almost the normal forms for oscillatory systems, where $\text{sign}(a_1)=-\text{sign}(a_2)$, a_2 and b_2 determine whether the periodicity is supercritical or subcritical and a_3 and b_3 determine the amplitude of the oscillations in x and y respectively. This will directly lead towards that which is to be proven. However, I will try to prove it from a general perspective. A Hopf bifurcation is crossed when two complex conjugate eigenvalues cross the imaginary axis. That is, while having a nonzero imaginary part, their real part changes sign. To assign conditions to this, we need to compute the Jacobian:

$$
J=\begin{pmatrix} a_2(a_3-x^2-y^2)-2a_2x^2 & a_1-2a_2xy \\ b_1-2b_2xy & b_2(b_3-x^2-y^2)-2b_2y^2 \end{pmatrix}
$$

and the subsequent eigenvalues:

$$
\begin{aligned}
\lambda_1 &= \frac{1}{2}(-\sqrt{(-a_2a_3+3a_2x^2+a_2y^2-b_2b_3+b_2x^2} \\
&\quad +3b_2y^2)^2-4(-a_1b_1+2a_1b_2xy+a_2a_3b_2b_3-a_2a_3b_2x^2 \\
&\quad -3a_2a_3b_2y^2+2a_2b_1xy-3a_2b_2b_3x^2-a_2b_2b_3y^2+ \\
&\quad 3a_2b_2x^46a_2b_2x^2y^2+3a_2b_2y^4)+a_2a_3-3a_2x^2-a_2y^2 \\
&\quad +b_2b_3-b_2x^2-3b_2y^2) \\
\lambda_2 &= \frac{1}{2}(\sqrt{(-a_2a_3+3a_2x^2+a_2y^2-b_2b_3+b_2x^2} \\
&\quad +3b_2y^2)^2-4(-a_1b_1+2a_1b_2xy+a_2a_3b_2b_3-a_2a_3b_2x^2 \\
&\quad -3a_2a_3b_2y^2+2a_2b_1xy-3a_2b_2b_3x^2-a_2b_2b_3y^2+ \\
&\quad 3a_2b_2x^46a_2b_2x^2y^2+3a_2b_2y^4)+a_2a_3-3a_2x^2-a_2y^2 \\
&\quad +b_2b_3-b_2x^2-3b_2y^2)
\end{aligned}
$$

For the eigenvalues, a solving algorithm is used. Note that we did not implement any coupling term yet, which might alter the third column of the Jacobian. We can see that under the following condition, λ_1 and λ_2 have a nonzero imaginary part and are subsequently complex conjugates:

$$
\begin{aligned}
G(x,y) &:= (-a_2a_3+3a_2x^2+a_2y^2-b_2b_3+b_2x^2+3b_2y^2)^2 \\
&\quad -4(-a_1b_1+2a_1b_2xy+a_2a_3b_2b_3-a_2a_3b_2x^2 \\
&\quad -3a_2a_3b_2y^2+2a_2b_1xy-3a_2b_2b_3x^2-a_2b_2b_3y^2 \\
&\quad +3a_2b_2x^4+6a_2b_2x^2y^2+3a_2b_2y^4)<0
\end{aligned}
$$

If this is held, the real part needs to switch sign to actually cross the Hopf bifurcation, indicating that

$$
H(x,y) := a_2a_3-3a_2x^2-a_2y^2+b_2b_3-b_2x^2-3b_2y^2
$$

crosses zero. We will now simplify this proof by realizing that system Eqn. 2 has a stationary solution $(x,y)=(0,0)$ and in case of periodic solutions, will oscillate around this equilibrium. This indicates that the Hopf bifurcation point (if it exists) is at $(x,y)=(0,0)$. This means that we can simplify

G and H:

$$\begin{aligned} G(0,0) &= (-a_2a_3 - b_2b_3)^2 - 4(-a_1b_1 + a_2a_3b_2b_3) \\ &= a_2^2a_3^2 - 2a_2a_3b_2b_3 + b_2^2b_3^2 + 4a_1b_1 \\ &= (a_2a_3 - b_2b_3)^2 + 4a_1b_1 \\ H(0,0) &= a_2a_3 + b_2b_3 \end{aligned}$$

For $G(0,0)$ to become negative, this in particular means $a_1b_1 < 0$. And for $H(0,0)$ to be negative (which it should be in the case of a stable equilibrium), $a_2a_3 + b_2b_3 < 0$ and it crosses a Hopf bifurcation if $a_2a_3 + b_2b_3 = 0$.

□

Acknowledgements. First and foremost, I thank prof. dr. ir. Henk Dijkstra and dr. Anna von der Heydt, who supervised me throughout the project. Our fortnightly meetings allowed for creative thinking and information-dense conversations which helped a lot when approaching a novel concept like cascading tipping. Furthermore, I thank the people from the IMAU institute, including fellow students, that assisted me with technical problems. Among them, I specifically thank ir. Michael Kliphuis, who helped me with gaining access to data of the ESSENCE project. Finally, I could not have written this Master's thesis without anybody to share my enthusiasm and frustration with. For this I thank my family, my friends and specifically Jolein Hondsmerk.

References

Aleina, F. C., Baudena, M., D'Andrea, F., and Provenzale, A.: Multiple equilibria on planet Dune: Climate-vegetation dynamics on a sandy planet, Tellus B, 65, http://www.tellusb.net/index.php/tellusb/article/view/17662, 2013.

Ashwin, P., Creaser, J., and Tsaneva-Atanasova, K.: Fast and slow domino effects in transient network dynamicss, http://arxiv.org/abs/1701.06148, 2017.

Barriopedro, D., García-Herrera, R., Lupo, A. R., and Hernández, E.: A Climatology of Northern Hemisphere Blocking, Journal of Climate, 19, 1042–1063, doi:10.1175/JCLI3678.1, http://dx.doi.org/10.1175/JCLI3678.1, 2006.

Bathiany, S., Dijkstra, H., Crucifix, M., Dakos, V., Brovkin, V., Williamson, M. S., Lenton, T. M., and Scheffer, M.: Beyond bifurcation: using complex models to understand and predict abrupt climate change, Dynamics and Statistics of the Climate System, 1, dzw004, doi:10.1093/climsys/dzw004, +http://dx.doi.org/10.1093/climsys/dzw004, 2016a.

Bathiany, S., van der Bolt, B., Williamson, M., Lenton, T., Scheffer, M., van Nes, E., and Notz, D.: Statistical indicators of Arctic sea-ice stability - prospects and limitations, The Cryosphere, 10, 1631–1645, dOI: 10.5194/tc-10-1631-2016, 2016b.

Charney, J. G. and DeVore, J. G.: Multiple Flow Equilibria in the Atmosphere and Blocking, Journal of the Atmospheric Sciences, 36, 1205–1216, doi:10.1175/1520-0469(1979)036<1205:MFEITA>2.0.CO;2, http://dx.doi.org/10.1175/1520-0469(1979)036<1205:MFEITA>2.0.CO;2, 1979.

Coxall, H. and Pearson, P.: The Eocene-Oligocene Transition, in: Deep-Time Perspectives on Climate Change: Marrying the Signal from Computer Models and Biological Proxies, The Micropalaeontological Society Special Publication, pp. 351–387, 2007.

Coxall, H., Wilson, P., Pälike, H., Lear, C., and Backman, J.: Rapid stepwise onset of Antarctic glaciation and deeper calcite compensation in the Pacific Ocean, Nature, 533, 53–57, doi:10.1038/nature03135, 2005.

Creaser, J., Tsaneva-Atanasova, K., and Ashwin, P.: Sequential noise-induced escapes for oscillatory network dynamics, http://arxiv.org/abs/1705.08462, 2017.

Dakos, V., Scheffer, M., van Nes, E. H., Brovkin, V., Petoukhov, V., and Held, H.: Slowing down as an early warning signal for abrupt climate change, Proceedings of the National Academy of Sciences, 105, 14 308–14 312, doi:10.1073/pnas.0802430105, http://www.pnas.org/content/105/38/14308.abstract, 2008.

DeConto, R. and Pollard, D.: Rapid Cenozoic glaciation of Antarctica induced by declining atmospheric CO_2, Nature, 421, 245–249, doi:10.1038/nature01290, 2003.

Dijkstra, H. and Weijer, W.: Stability of the global ocean circulation: basic bifurcation diagrams, Journal of Physical Oceanography, 35, 933–948, 2005.

Dijkstra, H. A. and Weijer, W.: Stability of the global ocean circulation: The connection of equilibria within a hierarchy of models, Journal of Marine Research, 61, 725–743, doi:doi:10.1357/002224003322981129, http://www.ingentaconnect.com/content/jmr/jmr/2003/00000061/00000006/art00002, 2003.

Ditlevsen, P. D. and Johnsen, S. J.: Tipping points: Early warning and wishful thinking, Geophysical Research Letters, 37, n/a–n/a, doi:10.1029/2010GL044486, http://dx.doi.org/10.1029/2010GL044486, l19703, 2010.

Dong, B. and Sutton, R.: Enhancement of ENSO Variability by a Weakened Atlantic Thermohaline Circulation in a Coupled GCM, Journal of Climate, 20, 4920–4939, doi:10.1175/JCLI4284.1, http://dx.doi.org/10.1175/JCLI4284.1, 2007.

Drijfhout, S., Bathiany, S., Beaulieu, C., Brovkin, V., Claussen, M., Huntingford, C., Scheffer, M., Sgubin, G., and Swingedouw, D.: Catalogue of abrupt shifts in Intergovernmental Panel on Climate Change climate models, Proceedings of the National Academy of Sciences, 112, E5777–E5786, doi:10.1073/pnas.1511451112, http://www.pnas.org/content/112/43/E5777.abstract, 2015.

Gildor, H. and Tziperman, E.: Sea ice as the glacial cycles' Climate switch: role of seasonal and orbital forcing, Paleoceanography, 15, 605–615, doi:10.1029/1999PA000461, http://dx.doi.org/10.1029/1999PA000461, 2000.

Gildor, H. and Tziperman, E.: A sea ice climate switch mechanism for the 100-kyr glacial cycles, Journal of Geophysical Research: Oceans, 106, 9117–9133, doi:10.1029/1999JC000120, http://dx.doi.org/10.1029/1999JC000120, 2001.

Gildor, H., Tziperman, E., and Toggweiler, J. R.: Sea ice switch mechanism and glacial-interglacial CO2 variations, Global Biogeochemical Cycles, 16, 6–1–6–14, doi:10.1029/2001GB001446, http://dx.doi.org/10.1029/2001GB001446, 2002.

Held, H. and Kleinen, T.: Detection of climate system bifurcations by degenerate fingerprinting, Geophysical Research Letters, 31, n/a–n/a, doi:10.1029/2004GL020972, http://dx.doi.org/10.1029/2004GL020972, l23207, 2004.

Hirota, M., Holmgren, M., Van Nes, E. H., and Scheffer, M.: Global Resilience of Tropical Forest and Savanna to Critical Transitions, Science, 334, 232–235, doi:10.1126/science.1210657, http://science.sciencemag.org/content/334/6053/232, 2011.

Huber, M. and Nof, D.: The ocean circulation in the southern hemisphere and its climatic impacts in the Eocene, Palaeogeography, Palaeoclimatology, Palaeoecology, 231, 9 – 28, doi:http://dx.doi.org/10.1016/j.palaeo.2005.07.037, http://www.sciencedirect.com/science/article/pii/S0031018205004785, antarctic Climate Evolution: geological records from the margin and modelling, 2006.

Huisman, S. E., Dijkstra, H. A., von der Heydt, A., and de Ruijter, W. P. M.: Robustness of multiple equilibria in the global ocean circulation, Geophysical Research Letters, 36,

n/a–n/a, doi:10.1029/2008GL036322, http://dx.doi.org/10.1029/2008GL036322, l01610, 2009.

Jungclaus, J. H., Haak, H., Esch, M., Roeckner, E., and Marotzke, J.: Will Greenland melting halt the thermohaline circulation?, Geophysical Research Letters, 33, n/a–n/a, doi:10.1029/2006GL026815, http://dx.doi.org/10.1029/2006GL026815, l17708, 2006.

Kutzbach, J., Bonan, G., Foley, J., and Harrison, S.: Vegetation and soil feedbacks on the response of the African monsoon to orbital forcing in the early to middle Holocene, Nature, 384, 623–626, doi:10.1038/384623a0, http://dx.doi.org/10.1038/384623a0, 1996.

Lenton, T. M. and Williams, H. T.: On the origin of planetary-scale tipping points, Trends in Ecology & Evolution, 28, 380 – 382, doi:http://dx.doi.org/10.1016/j.tree.2013.06.001, http://www.sciencedirect.com/science/article/pii/S0169534713001456, 2013.

Livina, V. and Lenton, T.: A modified method for detecting incipient bifurcations in a dynamical system, Geophysical Research Letters, 34, n/a–n/a, doi:10.1029/2006GL028672, http://dx.doi.org/10.1029/2006GL028672, l03712, 2007.

Pearson, P., Foster, G., and Wade, B.: Atmospheric carbon dioxide through the Eocene–Oligocene climate transition, Nature, 461, 1110–3, 2009.

Peng, C.-K., Buldyrev, S. V., Havlin, S., Simons, M., Stanley, H. E., and Goldberger, A. L.: Mosaic organization of DNA nucleotides, Phys. Rev. E, 49, 1685–1689, doi:10.1103/PhysRevE.49.1685, https://link.aps.org/doi/10.1103/PhysRevE.49.1685, 1994.

Podnobik, B. and Stanley, H.: Detrended Cross-Correlation Analysis: A New Method for Analyzing Two Non-stationary Time Series, 2007.

Scheffer, M., Bascompte, J., Brock, W., Brovkin, V., Carpenter, S., Dakos, V., Held, H., van Nes, E., Rietkerk, M., and Sugihara, G.: Early-warning signals for critical transitions, Nature, 461, 53–59, doi:10.1038/nature08227, 2009.

Stommel, H.: Thermohaline Convection with Two Stable Regimes of Flow, Tellus A, 13, http://www.tellusa.net/index.php/tellusa/article/view/9491, 1961.

Tantet, A., van der Burgt, F. R., and Dijkstra, H. A.: An early warning indicator for atmospheric blocking events using transfer operators, Chaos, 25, 036406, doi:http://dx.doi.org/10.1063/1.4908174, http://scitation.aip.org/content/aip/journal/chaos/25/3/10.1063/1.4908174, 2015.

Thompson, J. and Stewart, H.: Nonlinear Dynamics and Chaos, Wiley, https://books.google.nl/books?id=vQvu-5VPkmcC, 2002.

Thompson, J. M. T. and Sieber, J.: Predicting Climate Tipping as a noisy bifurcation: a review, International Journal of Bifurcation and Chaos, 21, 399–423, doi:10.1142/S0218127411028519, http://www.worldscientific.com/doi/abs/10.1142/S0218127411028519, 2011.

Tigchelaar, M., von der Heydt, A. S., and Dijkstra, H. A.: A new mechanism for the two-step δ^{18}O signal at the Eocene-Oligocene boundary, Climate of the Past, 7, 235–247, doi:10.5194/cp-7-235-2011, http://www.clim-past.net/7/235/2011/, 2011.

Timmermann, A., Jin, F., and Abshagen, J.: A Nonlinear Theory for El Niño Bursting, Journal of the Atmospheric Sciences, 60, 152–165, doi:10.1175/1520-0469(2003)060<0152:ANTFEN>2.0.CO;2, http://dx.doi.org/10.1175/1520-0469(2003)060<0152:ANTFEN>2.0.CO;2, 2003.

Timmermann, A., An, S.-I., Krebs, U., and Goosse, H.: ENSO Suppression due to Weakening of the North Atlantic Thermohaline Circulation, Journal of Climate, 18, 3122–3139, doi:10.1175/JCLI3495.1, http://dx.doi.org/10.1175/JCLI3495.1, 2005.

Timmermann, A., Okumura, Y., An, S.-I., Clement, A., Dong, B., Guilyardi, E., Hu, A., Jungclaus, J., Renold, M., Stocker, T., R.J., S., Sutton, R., Xie, S.-P., and Yin, J.: The Influence of a Weakening of the Atlantic Meridional Overturning Circulation on ENSO, Journal of Climate, 20, 4899–4919, doi:10.1175/JCLI4283.1, http://dx.doi.org/10.1175/JCLI4283.1, 2007.

Venzke, S., Latif, M., and Villwock, A.: The Coupled GCM ECHO-2., Journal of Climate, 13, 1371–1383, doi:10.1175/1520-0442(2000)013<1371:TCGE>2.0.CO;2, https://doi.org/10.1175/1520-0442(2000)013<1371:TCGE>2.0.CO;2, 2000.

Xie, S.-P., Miyama, T., Wang, Y., Xu, H., de Szoeke, S. P., Small, R. J. O., Richards, K. J., Mochizuki, T., and Awaji, T.: A Regional Ocean–Atmosphere Model for Eastern Pacific Climate: Toward Reducing Tropical Biases, Journal of Climate, 20, 1504–1522, doi:10.1175/JCLI4080.1, http://dx.doi.org/10.1175/JCLI4080.1, 2007.

Yuan, N., Zuntau, F. and, Z. H., Piao, L., Xoplaki, E., and Luterbacher, J.: Detrended Partial-Cross-Correlation Analysis: A New Method for Analyzing Correlations in Complex System, Scientific Reports, 5, doi:doi:10.1038/srep08143, 2015.

Zebende, G.: {DCCA} cross-correlation coefficient: Quantifying level of cross-correlation, Physica A: Statistical Mechanics and its Applications, 390, 614 – 618, doi:https://doi.org/10.1016/j.physa.2010.10.022, http://www.sciencedirect.com/science/article/pii/S0378437110008800, 2011.

Zebiak, S. E. and Cane, M. A.: A Model El Niño–Southern Oscillation, Monthly Weather Review, 115, 2262–2278, doi:10.1175/1520-0493(1987)115<2262:AMENO>2.0.CO;2, http://dx.doi.org/10.1175/1520-0493(1987)115<2262:AMENO>2.0.CO;2, 1987.

Zhang, D., Lee, T. N., Johns, W. E., Liu, C.-T., and Zantopp, R.: The Kuroshio East of Taiwan: Modes of Variability and Relationship to Interior Ocean Mesoscale Eddies, Journal of Physical Oceanography, 31, 1054–1074, doi:10.1175/1520-0485(2001)031<1054:TKEOTM>2.0.CO;2, http://dx.doi.org/10.1175/1520-0485(2001)031<1054:TKEOTM>2.0.CO;2, 2001.

Zhang, R. and Delworth, T. L.: Simulated Tropical Response to a Substantial Weakening of the Atlantic Thermohaline Circulation, Journal of Climate, 18, 1853–1860, doi:10.1175/JCLI3460.1, https://doi.org/10.1175/JCLI3460.1, 2005.

Zhou, W.: Multifractal detrended cross-correlation analysis for two nonstationary signals, Physical Review, 77, https://arxiv.org/abs/0803.2773v1, 2008.